Final Technical Report

for

Grant NCC 2-845
NASA - Ames Research Center

Grant Period:
1 January 1994 to 31 December 1995,
no-cost extension to 31 December 1996

Numerical Study of Boundary-Layer Control in Aerodynamics

Submitted by

Tom I-P. Shih
Department of Mechanical Engineering
Carnegie Mellon University
Pittsburgh, PA 15213-3890

21 July 1997

I. Introduction

This project was funded to perform three tasks. The first task is to study shock-wave boundary-layer interactions with bleed. This study is relevant to boundary-layer control in external and mixed-compression inlets of supersonic aircraft. The second task is to test RAAKE, a code developed for computing turbulence quantities. The third task is to compute flow around the Ames ER-2 aircraft that has been retrofitted with containers over its wings and fuselage.

In this report, the accomplishments made in each of the above three tasks are given in the sections below. Additional details are given in the Appendix in the form of publications.

II. Task 1: Shock-Wave/Boundary-Layer Interactions with Bleed

In this area, the following two studies were made. In the first study, a series of simulations were performed for the following problem: a supersonic turbulent, boundary layer flow next to a flat plate with a planar incident oblique shock wave that impinges over a bleed region in which the bleed into a plenum is through rows of circular holes that are arranged in a staggered fashion. These simulations investigated the effects of spacing between bleed holes in the streamwise and spanwise directions.

The results of this study are summarized in Ref. 1 (Ref. 1 is reproduced in the Appendix). Key findings are as follows: (1) A "barrier" shock was found to form in every hole by the bleed process itself if the plenum pressure is sufficiently low. (2) These "barrier" shocks were found to induce considerable disturbances above the plate. (3) When there are rows of holes arranged in a staggered fashion, bleeding through these holes exerted considerable spanwise influence which is contrary to single hole or holes in tandem cases. (4) For the range of bleed-hole spacings investigated, just two rows of holes were able to block the shock-induced adverse pressure gradient from propagating upstream. This indicates that judicious hole placement can greatly reduce the amount of bleed needed to control flow separation. (5) Both the streamwise and

spanwise spacings can exceed the hole diameter with the optimum value dependent upon the boundary-layer profile created by bleed and on the amount of adverse pressure gradient that profile can withstand before separating. This indicates that further optimization can be made by minimizing bleed per unit area.

In the second study, computations were performed to validate the computational procedure and examine the effects of two turbulence models. On computational procedure, validation is needed on the overlapped grid system used and on the OVERFLOW code used. On turbulence modeling, assessment is needed on the usefulness of the algebraic Baldwin-Lomax turbulence model and the one-equation model of Baldwin and Barth. The validation and assessment were made by comparing predicted results with measured ones reported by Willis, et al. (Ref. 2).

The outcome of the validation and assessment studies are summarized in Ref. 3 (Ref. 3 is reproduced in the Appendix). Key findings are as follows. On grid structure and code, OVERFLOW on an overlapped grids can provide very accurate results for both bleed rate and boundary-layer profile above the flat plate upstream and downstream of the bleed region. Note that this validation is for choked flow through 90-degree circular holes into a very big plenum. On the effects of turbulence models, the Baldwin-Lomax (B-L) model was found to produce accurate results for bleed rate as well as the boundary layer (BL) pitot-stagnation-pressure profiles on a grid that is relatively coarse in the streamwise direction provided separation bubbles on the flat plate are either non-existent or very small. With a finer grid, B-L was able to predict a larger separation bubble, one closer to the correct size. But, once B-L predicts a separation bubble that is sufficiently large, then results predicted downstream of it become less satisfactory. If B-L does not predict separation though one exists, then the predicted bleed rate was lower than should be but the predicted pitot-stagnation pressure downstream of the bleed region was found to be accurate. Though Baldwin-Barth turbulence model can predict flow separation on the flat plate with a relatively coarse grid in the streamwise direction, it too does not provide satisfactory results for this problem if there is flow separation.

III. Task 2: Development of the RAAKE Code

RAAKE was developed under a previous grant with NASA Ames (NAG 2-709). RAAKE contains the following two-equation turbulence models: two-layer model of Chen and Patel, low Reynolds number k-ε model of Jones and Launders, a RNG k-ε model, and a k-ω model. The discretization was as follows: first- or second-order accurate in time implicit formula (i.e., Euler implicit or three-point backward), first- or second-order upwind based on flux-vector splitting for the inviscid terms, and second-order central differencing for the diffusion terms. The algorithm used to obtain solutions to the system of equations that result from the discretization was an LU algorithm with novel treatment of diffusion and source terms as described in Refs. 4 and 5.

During the grant period, the following efforts were made to test RAAKE. First, run RAAKE decoupled from OVERFLOW; i.e., take a converged solution from OVERFLOW for a boundary-layer flow in terms of the conserved variables (i.e., ρ, ρu, ρv, ρw, and e) that was obtained by using the Baldwin-Lomas model and then use that to compute k and ε or k and ω. RAAKE running in this mode was found to very robust and quickly yielded converged solutions. Also, it was found to give accurate results in terms of profiles for the turbulence quantities. Next, RAAKE was coupled with OVERFLOW to simulate the following two problems by using the low Reynolds number k-ε model of Jones and Launders: (1) supersonic boundary-layer flow past a compression corner and (2) subsonic flow past a backward facing step. For the compression corner flow, RAAKE was reasonably robust but yielded poor quality results. The poor quality results may be due to the turbulence model used. For the backward-facing step problem, RAAKE performed very badly by being not very robust. In fact, the time-step size needed in order to obtain stable solutions with OVERFLOW was exorbitantly small. Since only a part of the first year of this grant was devoted to RAAKE, efforts to improve RAAKE were not carried out.

IV. Task 3: Simulation of Flow over the Ames ER-2 Aircraft

During the second year of the grant, the focus shifted to the Ames ER-2 aircraft. Basically, the Ames ER-2 aircraft was being retrofitted by having oval-shaped containers mounted above the fuselage and on the wings. These containers, known as starlinks and pods, house antennas, probes, computers, and communication equipment. The objective was to compute flow past this retrofitted aircraft to understand (1) how boundary layers and wakes induced by the containers affect the overall aerodynamics of the aircraft and (2) the accuracy in data acquisition from flow disturbances caused by the containers as well as the aircraft itself about probe regions.

Unlike the earlier two tasks, this task was carried out at NASA Ames by Mark J. Rimlinger (a Carnegie Mellon graduate student who was sent to work at NASA Ames in 1995) with guidance from Wei J. Chyu and Andrew C. Roberts of NASA Ames. Thus, all efforts on this task were carried by Mark Rimlinger, Wei J. Chyu, and Andrew C. Roberts. During 1995, the following simulations were completed: (1) flow past a wing with pod, (2) flow past a wing with pod fitted with a camera window, (3) flow past a wing with pod fitted with a recess cavity, (4) flow past a wing with pod that had an inlet for through flow, (5) flow past a complete ER-2 aircraft (with fuselage, wing, inlet, and boundary-layer diverter) except for the tail, (6) repeat 5 except replace standard wing with extended wing, and (7) repeat 5 except replace wing with spiroid wing. Though no publications were results, many presentations were made to Lockheed and NASA. Please see Mark J. Rimlinger, Wei J. Chyu, or Andrew C. Roberts of NASA Ames for these.

References

1. Rimlinger, M.J., Shih, T.I-P., and Chyu, W.J., "Three-Dimensional Shock-Wave/Boundary-Layer Interactions with Bleed through Rows of Holes," AIAA Journal of Propulsion and Power, Vol. 12, No. 2, 1996, pp. 217-224.

2. Willis, B.P., Davis, D.O., and Hingst, W.R., "Flowfield Measurements in a Normal-Hole-Bled Oblique Shock-Wave and Turbulent Boundary-Layer Interaction," AIAA 95-2885, July 1995.

3. Rimlinger, M.J., Shih, T.I-P., Chyu, W.J., Willis, B.P., Davis, D.O., "Computations of Shock-Wave/Boundary-Layer Interactions with Bleed," AIAA Paper No. 96-0432, presented at the 34th AIAA Aerospace Sciences Meeting, January 15-18, 1996, Reno, Nevada.

4. Shih, T.I-P. and Chyu, W.J., "Approximate-Factorization with Source Terms," AIAA Journal, Vol. 29, 1991, pp. 1759-1760.

5. Shih, T.I-P., Steinthorsson, E., and Chyu, W.J., "Implicit Treatment of Diffusion Terms in Lower-Upper Algorithms," AIAA Journal, Vol. 31, No. 4, 1993, pp. 788-791.

APPENDIX

Shock-Wave/Boundary-Layer Interactions with Bleed Through Rows of Holes

M. J. Rimlinger, T. I-P. Shih, W. J. Chyu

Reprinted from

Journal of Propulsion and Power

Volume 12, Number 2, Pages 217–224

AIAA

A publication of the
American Institute of Aeronautics and Astronautics, Inc.
370 L'Enfant Promenade, SW
Washington, DC 20024-2518

JOURNAL OF PROPULSION AND POWER
Vol. 12, No. 2, March–April 1996

Shock-Wave/Boundary-Layer Interactions with Bleed Through Rows of Holes

M. J. Rimlinger* and T. I-P. Shih†
Carnegie–Mellon University, Pittsburgh, Pennsylvania 15213-3890
and
W. J. Chyu‡
NASA Ames Research Center, Moffett Field, California 94035

Computations were performed to investigate three-dimensional, shock-wave/boundary-layer interactions on a flat plate with bleed through four staggered rows of circular holes that discharge into the same plenum. The focus of the computations was to examine how bleed through rows of holes affect bleed rate and the pressure and Mach number distributions. The effects of the following parameters on the flow were investigated: 1) with and without shock-wave impingement on the boundary layer and 2) spacings between bleed holes in the streamwise and spanwise directions. Results show that just two rows of bleed holes arranged in a staggered fashion placed upstream of the incident shock are adequate in blocking the shock-induced adverse pressure gradient from propagating further upstream. Results also show that the spacings between the centers of holes can exceed the hole diameter not just in the streamwise direction, but also in the spanwise direction, and still be able to control shock-induced flow separation. This study is based on the ensemble-averaged, "full compressible" Navier–Stokes (N–S) equations closed by the Baldwin–Lomax algebraic turbulence model. Solutions to the ensemble-averaged N–S equations were obtained by an implicit, partially split, two-factored algorithm with flux-vector splitting in the streamwise direction on a chimera overlapping grid.

Introduction

SHOCK-WAVE/BOUNDARY-LAYER interactions and their effective control play an important role in the operation of mixed-compression supersonic inlets. These inlets utilize shock waves to reduce the incoming air from supersonic to subsonic speeds for the compressor. But, the many reflected shock waves within the inlet thicken boundary layers and cause flow distortions. Also, if the shock waves are sufficiently strong, then boundary-layer separation takes place, which can lead to the unstart condition.

One effective way of controlling the unfavorable effects produced by shock waves is to place bleed holes in regions where shock waves impinge on the boundary layer. The importance of bleed in controlling shock-wave/boundary-layer interactions has led a number of investigators to use both experimental and numerical methods to study this problem.[1,2] According to Hamed and Shang,[2] though all experimental studies agree that bleed can control shock-wave/boundary-layer interactions, they disagree on how bleed-hole geometric and operating parameters influence the effectiveness of the bleed process. These discrepancies indicate the complexities of the flow in the region about bleed holes. In that region, many parameters can affect the flow with different ones dominating under different conditions.

Numerical studies of shock-wave/boundary-layer interactions with bleed fall into two groups. One group models the bleed process by using boundary conditions and/or a roughness model without resolving the flow through the bleed holes.[3-7] The advantage of this approach is that it is more efficient computationally, which enables a complete inlet configuration to be simulated, as was done in Refs. 4 and 7. The other group studies the bleed process by resolving the flow through each bleed hole.[8-17] The advantage of this approach is that it can reveal the nature of the flow governing the bleed process. The understanding gained by these studies can guide the construction of boundary conditions and roughness models used by the first group.

Hamed et al.,[8-12] Hahn et al.,[13] and Omi et al.[14] performed two-dimensional numerical studies of the flow in and around bleed holes. These studies modeled the bleed holes as slots. Hamed et al.[8-12] studied supersonic boundary-layer flow past a flat plate with an incident oblique shock wave. Their studies resolved the flow above the plate and in the bleed hole or holes. Hahn et al.[13] studied the same problem, except the flow in the plenum was resolved as well. Omi et al.[14] studied an entire inlet configuration with a single-hole bleed system at the inlet's throat.

Though the aforementioned two-dimensional studies provided valuable insights into the bleed process, realistic bleed holes are three dimensional instead of two dimensional. Rimlinger et al.,[15] Shih et al.,[16] and Chyu et al.[17] performed three-dimensional numerical studies of shock-wave/boundary-layer interaction on a flat plate with bleed through circular holes connected to a plenum. Rimlinger et al.[15] and Shih et al.[16] showed how bleed-hole placement relative to shock-wave impingement affected upstream, spanwise, and downstream influence lengths. These studies also showed that if the pressure in the plenum is sufficiently low, then the bleed process forms a "barrier" shock in and on the downstream edge of each bleed hole. The authors noted that this barrier shock can block information downstream of it from propagating upstream, and hence, is a mechanism that can be utilized to prevent flow separation in addition to the mechanism of removing low

Presented as Paper 94-0313 at the AIAA 32nd Aerospace Sciences Meeting and Exhibit, Reno, NV, Jan. 10–13, 1994; received July 18, 1994; revision received June 5, 1995; accepted for publication June 6, 1995.

*Graduate Student, Department of Mechanical Engineering.
†Professor, Department of Mechanical Engineering. Member AIAA.
‡Research Scientist, Applied Aerodynamics Branch. Member AIAA.

momentum air next to solid surfaces. In order to utilize the barrier shock, the authors suggested that bleed holes be located slightly upstream of the location where the incident shock wave impinges on the subsonic part of the boundary layer. This is so that the barrier shock is formed upstream of any disturbances created by the impinging shock. Shih et al.[16] further noted that the barrier shock also increases mixing in the spanwise direction because it disrupts the flow locally by slowing it down and increasing its static pressure. This increased mixing is still another mechanism that can be utilized to prevent flow separation and control flow distortions. Chyu et al.[17] showed in detail the bleed rate as well as the formation and structure of the barrier shock as a function of bleed-hole angle (30-deg slanted and 90-deg normal to the freestream direction), number of bleed holes (one or three in tandem), and pressure ratio across the bleed hole.

In the aforementioned three-dimensional studies, the focus was on shock-wave/boundary-layer interactions on a flat plate with bleed through either a single circular hole or three circular holes in tandem along the streamwise direction. So far, no one has investigated bleed through rows of holes (i.e., multiple holes in both the streamwise and the spanwise directions). Since these are the hole configurations used in practice, the objective of this investigation is to study shock-wave/boundary-layer interactions on a flat plate with bleed through four staggered rows of circular holes that discharge into the same plenum. The focus is to examine the effects of the following parameters on the flow: with and without shock-wave impingement on the boundary layer and spacings between bleed holes in the streamwise and spanwise directions.

In the next section, the shock-wave/boundary-layer interaction problem studied is described. Afterwards, the formulation, numerical method of solution, and results obtained are presented.

Description of Problem

A schematic diagram of the problem studied is shown in Fig. 1. It involves a supersonic turbulent boundary layer flowing past a flat plate with an incident oblique shock wave, bleed of the boundary layer through four rows of circular holes arranged in a staggered fashion, and a plenum where the bleed is discharged. All dimensions are given in terms of D, the diameter of all bleed holes, which is 0.2 in. For this problem, the domain is the region bounded by the dashed lines that includes the region above the flat plate, the plenum, and four "half" bleed holes. Only four half bleed holes are included because of symmetry in the spanwise direction.

For this problem, the fluid that enters the domain above the flat plate is air with a constant specific-heats ratio γ of 1.4. The freestream Mach number M_∞, static pressure P_∞, and

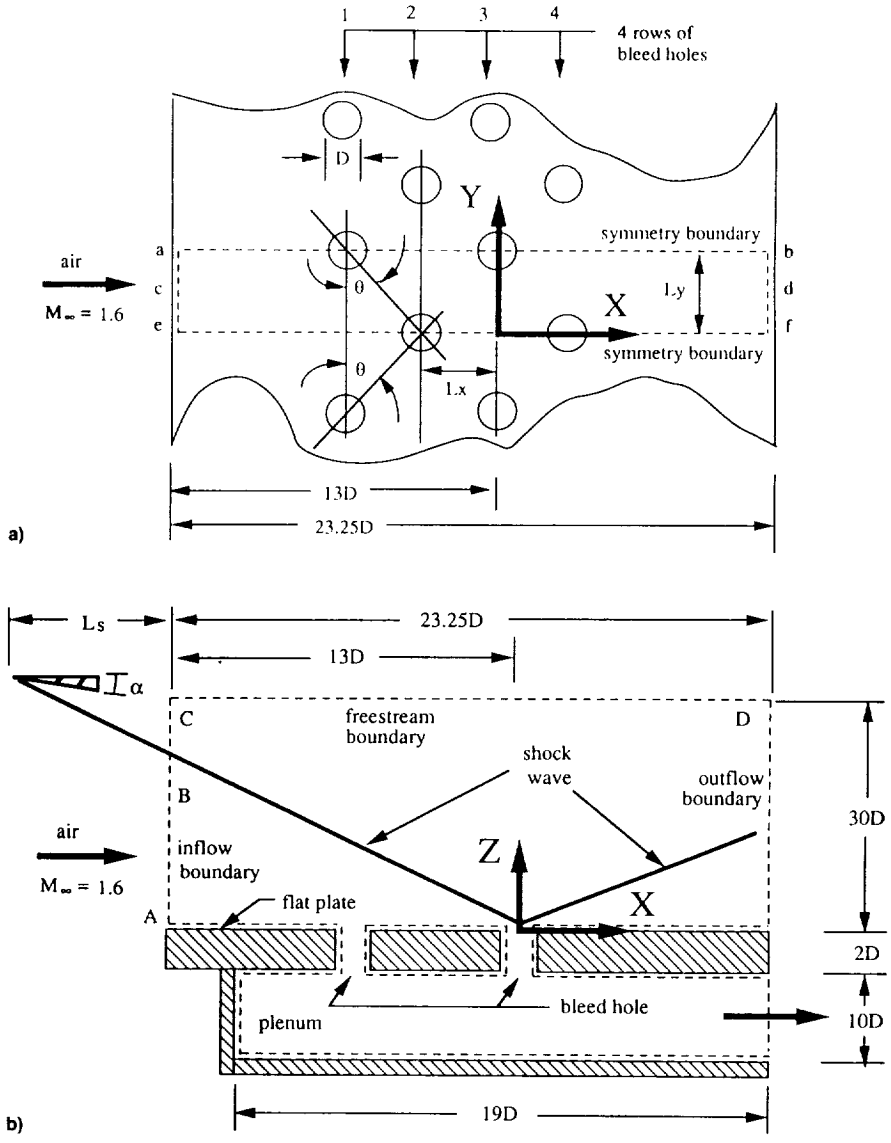

Fig. 1 Schematic diagram of bleed-hole problem: a) top view and b) side view along cross section a-b.

Table 1 Summary of cases studied[a]

Case no.	θ, deg	L_y	Shock?[b]
1	60	D	No
2	60	D	Yes
3	60	$1.5D$	Yes
4	70	D	Yes

[a]For all cases, $M_\infty = 1.6$, $P_\infty = 61.32$ kPa, $T_0 = 300$ K, $D = 0.2$ in., and $L_x = L_y \tan(\theta)$; see Fig. 1.
[b]When there is a shock, the shock would impinge or strike at the center of the bleed holes in the third row under inviscid conditions.

stagnation temperature T_0 are 1.6, 61.32 kPa, and 300 K, respectively. This supersonic flow has a turbulent, boundary layer next to the flat plate. At the inflow boundary, the thickness of that boundary layer δ is 0.6 in., which is equal to three times the diameter of the bleed holes. To induce flow of air through the bleed holes, the back pressures P_b at the exit of the plenum is maintained at $0.35P_\infty$.

A shock-wave generator characterized by L_x and α can cause an oblique shock wave to strike the turbulent, boundary layer on the flat plate. Computations were performed with and without this shock. When there is this shock, α was set at 7.5 deg, which produced a shock wave that was strong enough to induce flow separation on the flat plate in the absence of bleed. L_x was chosen so that the shock would incident on the flat plate at a distance of $13D$ measured from the inflow boundary under inviscid flow conditions (i.e., zero boundary-layer thickness).

Aside from investigating the bleed process with and without an incident shock, two aspects of the bleed-hole geometry were investigated, the angle θ and the distance (L_y and $L_x = L_y \tan\theta$) between adjacent holes (see Fig. 1a). The angles investigated are $\theta = 60$ and 70 deg. When $\theta = 60$ deg, the distance between all adjacent bleed holes is the same. When $\theta = 70$ deg, holes in the spanwise direction are closer than those in the streamwise direction. At $\theta = 60$ deg, two distances between bleed holes were investigated, $L_y = D$ and $1.5D$ [recall $L_x = L_y \tan(\theta)$]. At $\theta = 70$ deg, only one distance between bleed holes was investigated, $L_y = D$. Thus, three different arrangements of the four rows of bleed holes are investigated. For all three arrangements, the bleed holes are positioned so that the distance between the inflow boundary and a line that passes through the centers of the bleed holes in the third row (see Fig. 1a) is $13D$. Thus, when there is an incident shock, it would strike at the center of the bleed holes in the third row under inviscid conditions. All cases studied are summarized in Table 1.

Formulation of Problem

The flow problem described in the previous section was modeled by the density-weighted, ensemble-averaged conservation equations of mass, momentum ("full compressible" Navier–Stokes), and total energy written in generalized coordinates and cast in strong conservation-law form. The effects of turbulence were modeled by the Baldwin–Lomax algebraic turbulence model.[18]

To obtain solutions to the conservation equations, boundary and initial conditions are needed. The boundary conditions (BCs) employed in this study for the different boundaries shown in Fig. 1 were as follows. At the inflow boundary where the flow is supersonic everywhere except for a very small region next to the flat plate, two types of BCs were imposed. Along segment A-B, all flow variables were specified at the freestream conditions except for the streamwise velocity (which had a turbulent boundary-layer next to the flat plate), and the static temperature (which varied in the boundary layer to maintain a constant stagnation pressure). The velocity in the turbulent boundary layer was described by the van Driest profile when $y^+ < 50$ and by the one-seventh power-law profile when $50 \le y^+ \le y^+(\delta)$. Along segment B-C, postshock conditions based on inviscid oblique shock-wave theory were specified. These post-shock conditions were also specified along the freestream boundary (segment C-D). At the outflow boundary where the reflected shock wave exited the computational domain, the flow is also mostly supersonic except for a small region next to the flat plate so that all flow variables were extrapolated. Here, linear extrapolation based on three-point, backward differencing was employed. The BCs imposed at the two symmetry boundaries were zero derivatives of the dependent variables except for the velocity component normal to those boundaries that was set equal to zero. At the exit of the plenum where the flow is subsonic, a back pressure P_b was imposed, and density and velocity were extrapolated in the same manner as the variables at the outflow boundary. At all solid surfaces, the no-slip condition, adiabatic walls, and zero normal-pressure gradient were imposed.

Even though only steady-state solutions were of interest, initial conditions were needed because the unsteady form of the conservation equations was used. The initial conditions employed in this study were as follows. In the region above the flat plate, the initial condition was the two-dimensional, steady-state solution for an incident and a reflected oblique shock wave on a flat plate based on inviscid oblique shock-wave theory. The streamwise velocity profile, however, was modified to give the van Driest/one-seventh power-law profile. This necessitated the density and static temperature to be modified as well in order to maintain constant stagnation temperature in the boundary layer. The initial conditions used in the bleed hole and plenum were stagnant air at constant stagnation temperature T_0 and static pressure P_b.

Numerical Method of Solution

Solutions to the ensemble-averaged conservation equations of mass, momentum, and total energy closed by the Baldwin–Lomax algebraic turbulence model described in the previous section were obtained by using the Overflow code.[19] The Overflow code contains many algorithms. The one used in this study is as follows: inviscid flux-vector terms in the ξ-direction were upwind differenced by using the flux-vector splitting procedure of Steger and Warming.[20] Inviscid flux-vector terms in directions normal to the ξ direction were centrally differenced in order to reduce artificial dissipation in those directions. Diffusion terms in all directions were also centrally differenced. The time-derivative terms were approximated by the Euler implicit formula since only steady-state solutions are sought here. The system of nonlinear equations that resulted from the aforementioned approximations to the space and time derivatives were analyzed by using the partially split method of Steger et al.[21]

For the bleed-hole problem shown in Fig. 1 and summarized in Table 1, the computational domain is divided into six zones, one above the plate, one for each of the four half bleed holes, and one for the plenum. Each zone has a different coordinate system in order to align upwind differencing with the streamwise direction. For this six-zone computational domain, a chimera overlapped grid system is employed. Figure 2 shows an example of the chimera grid system used in the region around the bleed holes. Note that in this and all subsequent figures, the spatial dimensions X, Y, and Z are all nondimensionalized by $23.25D$.

For the zone above the flat plate, the grid system used was a single solution-adapted H-H grid (adaptation was based on the initial conditions), which has grid points clustered near the flat plate, bleed holes, and the impinging and reflected shock waves. The number of grid lines used in this H-H grid is as follows: 335 from inflow to outflow and 101 from plate surface to freestream boundary. Between the two symmetry boundaries, the number of grid lines differed depending upon L_y, it is 29 when $L_y = D$ (cases 1, 2, and 4 in Table 1), and 41 when $L_y = 1.5D$ (case 3). The grid spacings corresponding

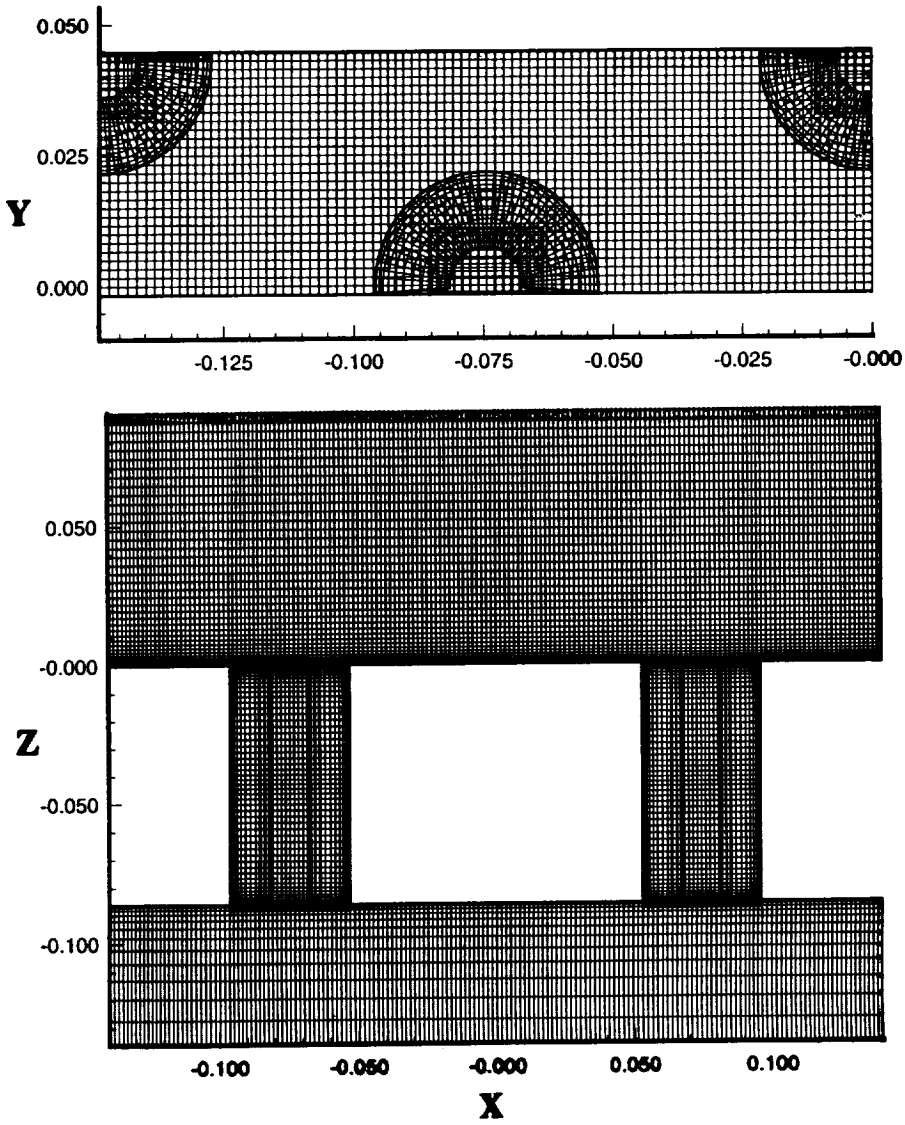

Fig. 2 Grid system near the bleed holes.

to 335 × 101 × 29 or 335 × 101 × 41 grid points are as follows. In the streamwise direction, they vary from $0.5D$ at the inflow boundary to $0.04D$ at a distance of $7.375D$ before where the shock wave would impinge on the plate under inviscid conditions. From $7.375D$, before the inviscid-shock-impingement point, to $4.625D$ after that point, the grid spacings are kept constant at $0.04D$. From $4.625D$ after the shock impingement point to the outflow boundary, they vary from 0.04 to $0.5D$. In direction normal to the plate, the grid spacings vary from $4 \times 10^{-6}D$ at the plate to $0.45D$ at the edge of the boundary layer. The grid points closest to the wall have y^+ values less than unity. The total number of grid points in the boundary layer is about 50. From the edge of boundary layer to the freestream boundary, they vary from 0.45 to $0.75D$. In the spanwise direction, the grid spacings are kept constant at $0.0385D$ and that is why the number of grid points is higher when L_z is larger. Here, it is noted that the grid spacings in the H-H grid above the plate are the same for all cases studied (i.e., cases 1–4) in order to ensure identical flow above the plate in the absence of bleed.

For each zone containing a bleed hole, two overlapping grids were used, an O-H grid touching the wall of the bleed hole and an H-H grid at the center of the bleed hole. The O-H grid with 62 × 47 × 11 grid points is used to resolve the circular geometry of the bleed hole. The H-H grid with 62 × 10 × 15 grid points is used to eliminate the centerline singularity associated with the O-H grid. Note that the grids in the bleed hole overlap the grid in the plenum by four grid lines, whereas they overlap the grid above the flat plate by only two grid lines. The reason for extending the bleed-hole grids further into the plenum is to accelerate convergence rate to steady state. Since BCs on overlapped boundaries are of the Dirichlet type and density-based algorithms such as the one used here have a slow convergence rate at low Mach numbers, information transfer between overlapped grids is slow if the initial conditions involved stagnant flow in both overlapped grids and if the spacings between the boundaries of the two overlapped grids are small.

For the zone containing the plenum, a single H-H grid was used. This H-H grid has either 335 × 29 × 51 or 335 × 41 × 51 grid points, depending upon L_z. The grid points are clustered near walls and bleed holes.

The grid system described previously was generated by using algebraic grid generation with one-dimensional stretching functions. Grid spacings in different grids were made comparable in regions where they overlapped in order to minimize aliasing error. The clustering and the number of grid points employed in each zone were determined by numerical experiments to ensure the following. First, the grid must be able to discern effects of the bleed holes on shock-wave/boundary-layer interactions. This required crisp resolution of the incident and reflected shock waves above the plate as well as the

shock structure in the bleed holes. Second, qualitative features of the predicted flowfield and the quantitative data obtained for the bleed rate are grid independent.

During computations, the flowfield in each grid was analyzed one at a time in the following order: 1) the H-H grid above the flat plate, 2) the H-H grid in the bleed hole, 3) the O-H grid in the bleed hole, 4) repeat 2 and 3 for all bleed holes, and 5) the H-H grid in the plenum. Information from one grid was passed to another grid via trilinear interpolation at grid boundaries. The required interpolation coefficients were obtained by using the Pegsus code.[22] This process of analyzing the flow in one grid at a time until all grids are analyzed was repeated for each time step until a converged solution was obtained.

Results

Numerical solutions were obtained to investigate shock-wave/boundary-layer interactions with bleed for the problem described and formulated in the previous sections and depicted in Fig. 1. The focus was to study pressure and Mach number distributions about the bleed holes with and without an incident shock and with two different parameters governing

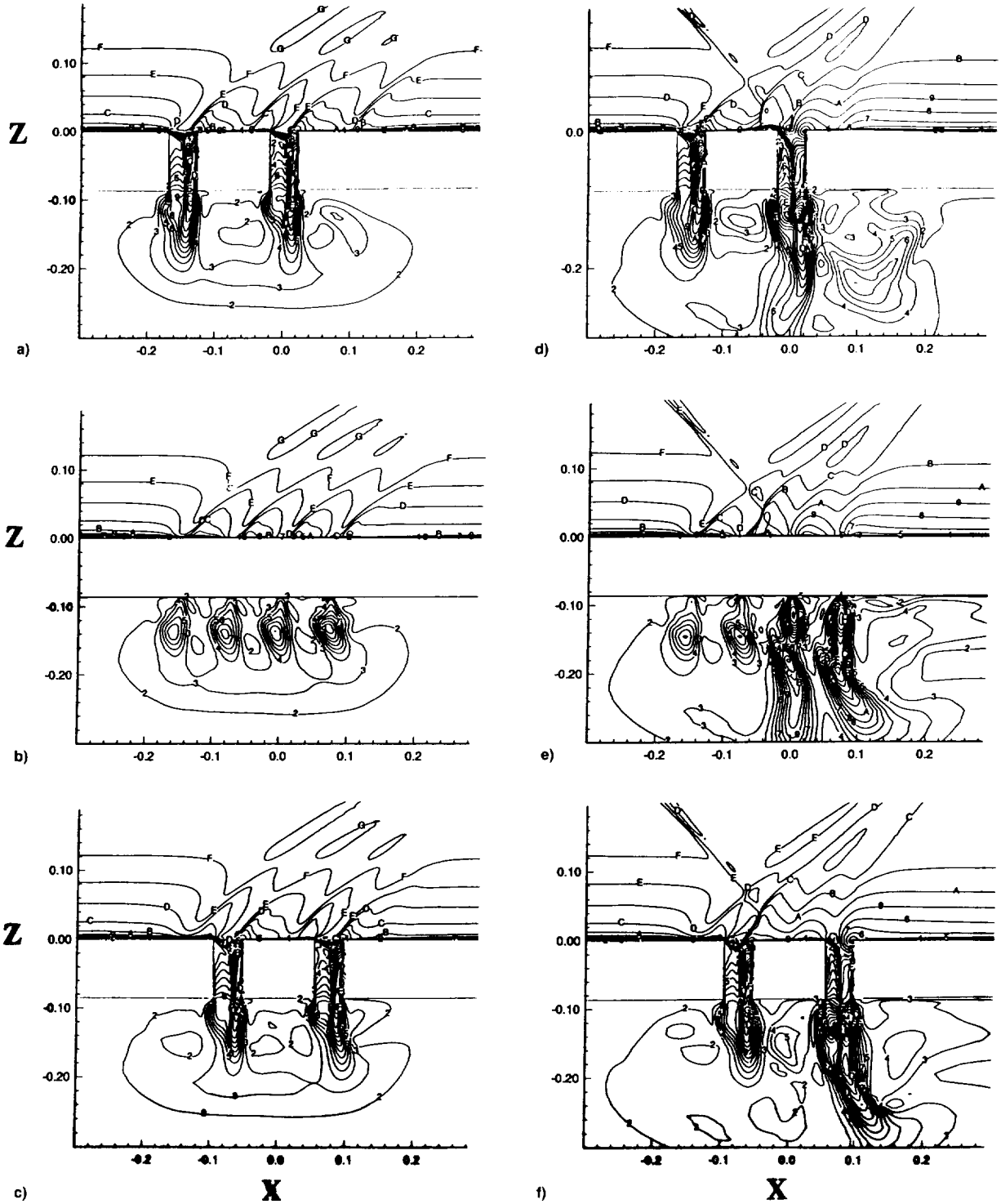

Fig. 3 Mach number contours (side view): a), b), and c) without incident shock (case 1); d), e), and f) with incident shock (case 2); a) and d) along a-b; b) and e) along c-d; and c) and f) along e-f.

staggered-hole arrangements, the angle θ and the distance between bleed holes L_s (see Fig. 1). A summary of the cases studied is given in Table 1.

Results are given in Figs. 3–6. Figure 3 shows Mach number contours with and without an incident shock (cases 1 and 2 in Table 1) along three planes perpendicular to the plate. Figure 4 shows the surface pressure for those two cases as well as a case that was computed with incident shock, but without bleed. Figure 5 shows pressure contours on the plate surface for all four cases. Though the bleed holes are not marked, they can be discerned by the pressure fields induced by them (e.g., the barrier shocks). Figure 6 gives the flow coefficient for each bleed hole. The flow coefficient is defined as the actual bleed rate divided by the ideal bleed rate with the ideal bleed rate being sonic flow through the entire bleed hole at freestream stagnation temperature and pressure. For the conditions of this study, the ideal bleed rate is 0.01233 kg/s.

Effects of Incident Shock

From Figs. 3a–3c and 4a, it can be seen that even without an incident shock (case 1), the bleed process itself creates a barrier shock in each bleed hole. These figures also show that without an incident shock, all barrier shocks have a similar structure, although those in rows 3 and 4 are slightly stronger than those in rows 1 and 2. The following observations can

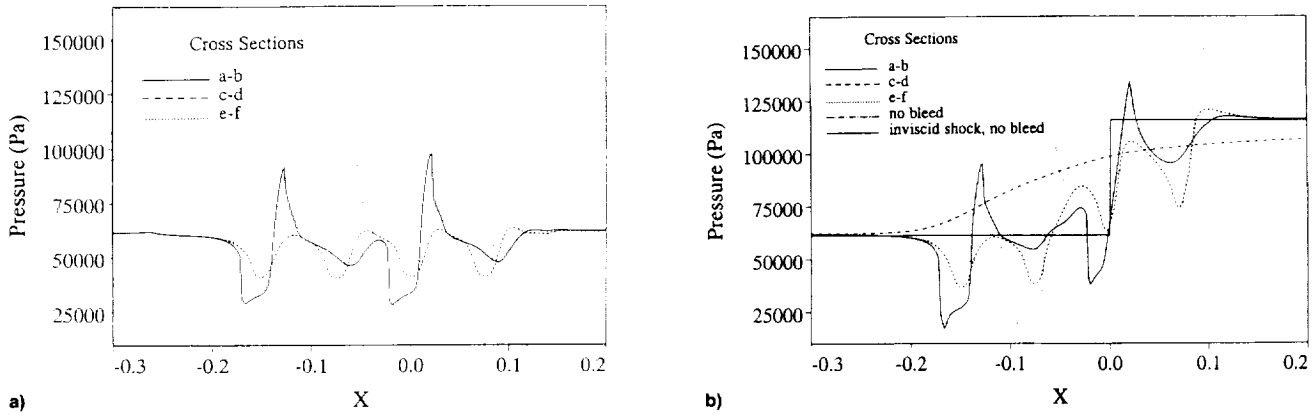

Fig. 4 Pressure along plate surface: a) without incident shock (case 1) and b) with incident shock (case 2).

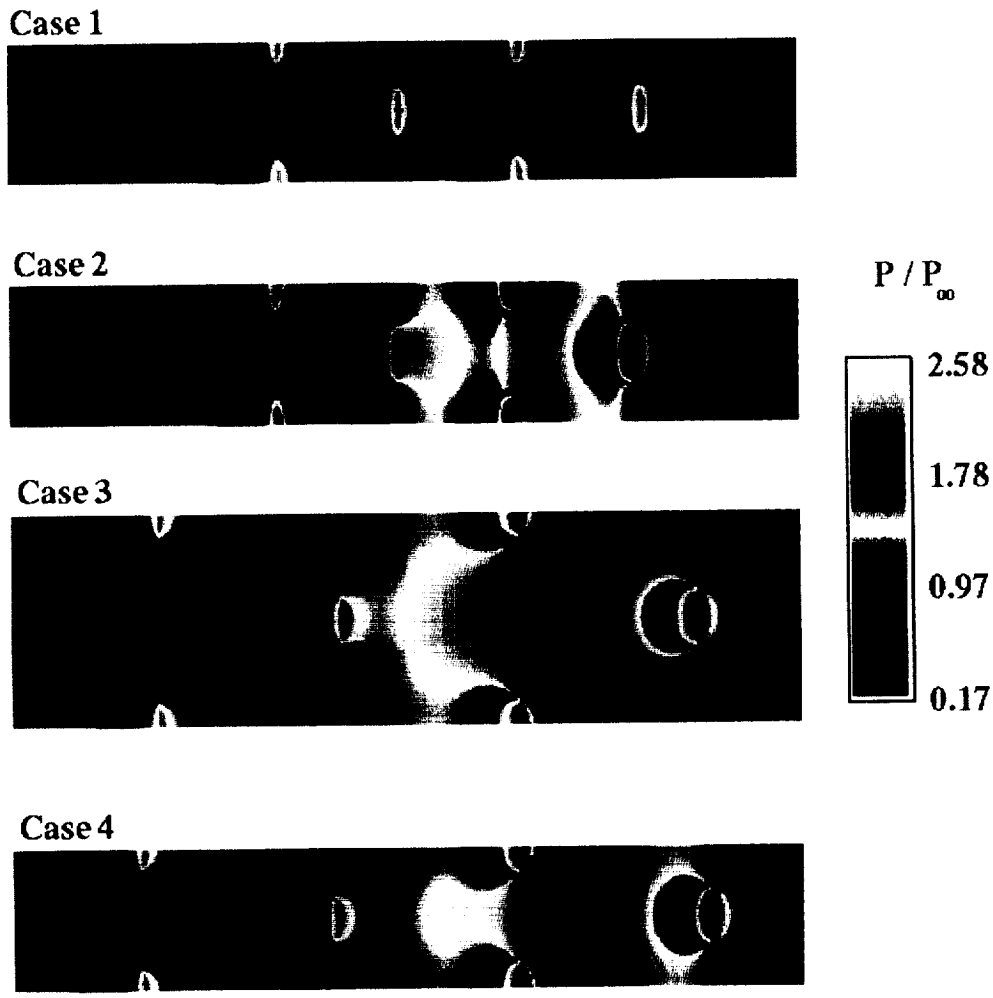

Fig. 5 Pressure contours on plate surface for all four cases.

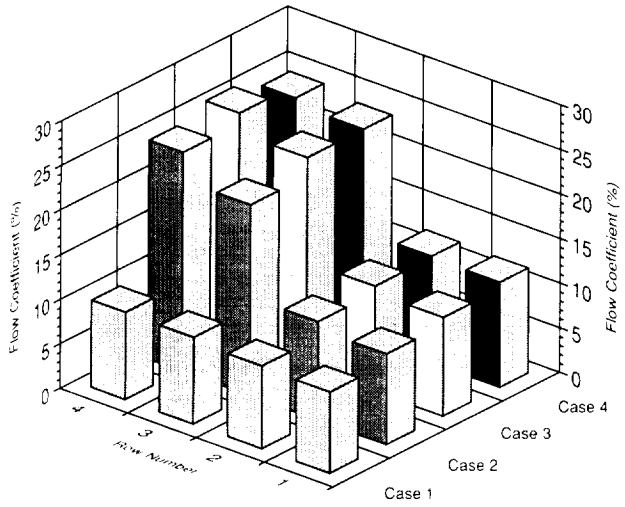

Fig. 6 Flow coefficient through each bleed hole.

be inferred from Figs. 3a–3c about the nature of the flow above the plate, in the bleed holes, and in the plenum. First, the barrier shocks set up considerable disturbances in the flow above the flat plate that extend beyond the thickness of the approaching boundary layer. Second, there is a large separated region in each bleed hole. Third, the jets issuing through the bleed holes into the plenum all have similar penetration depths and only weakly interact with each other. The weak interactions between the jets in the plenum can also be inferred from the pressure in the plenum. Though not shown here (see Ref. 23), the static pressure in the region between the jets in the plenum is nearly the same.

Figures 3d–3f and 4b show that with an incident shock (case 2), the structures of the flow upstream of that shock are almost identical to those for the case without the incident shock (case 1). After where the incident shock impinged on the boundary layer (which is slightly upstream of the bleed holes in the third row), the Mach number and pressure contours begin to differ considerably from the case without the incident shock. The most pronounced differences are as follows. First, barrier shocks in rows 3 and 4 are much stronger than those in rows 1 and 2 for obvious reasons. Second, the jets issuing through bleed holes in rows 3 and 4 penetrated much deeper into the plenum than those in rows 1 and 2. This is because the incident shock increased the amount of bleed by increasing the density and static temperature of the flow above the flat plate and by reducing the size of the separation bubble in the bleed holes. Third, jets issuing through bleed holes in rows 3 and 4 interact. These interactions affect the structure of the jet in the bleed hole and in the plenum, and hence, the bleed rate. At this point, it is interesting to note that despite the aforementioned differences, the disturbances in the flow above the plate created by bleed with and without the incident shock appear to be of similar magnitude.

Figure 5 shows differences created by an incident shock in terms of surface pressure. Without an incident shock (case 1), the following observations can be made. First, the surface pressure reduces as the flow approaches each bleed hole; reaches a minimum in regions between bleed holes in the spanwise direction; and then increases again until approaching another bleed hole. The minimum pressure region between the bleed holes in the spanwise direction arises because the flow above the plate is highly accelerated towards the holes by Prandtl–Meyer expansion waves, which lower static pressure. Second, the region of minimum pressure between the bleed holes has a chevron shape and it connects holes in the spanwise direction. This indicates that when there are rows of holes arranged in a staggered fashion, each bleed hole exerts considerable spanwise influence. This is in sharp contrast with the results obtained for a single bleed hole[16] and three holes along the streamwise direction.[17] Third, though not shown, the pressure gradients on the plate surface correspond to the following shear stresses that reflect on the fullness of the boundary layers above the surface (i.e., the higher the shear, the fuller the boundary layer, and vice versa):

1) Shear stress is highest in the region just downstream of each bleed hole because low momentum fluid was just bled and because of the strong favorable pressure gradient induced by the barrier shock.

2) Shear stress is lowest in regions between the barrier shocks in the spanwise direction because of the adverse pressure gradient that they induce.

3) In the spanwise direction, shear stress oscillates between high (downstream of a hole) and low (downstream of a between-hole region). With an incident shock, Fig. 5 (case 2) shows the following: first, holes in row 2 can be seen to block effectively (though not completely as described later) the adverse pressure gradient created by the incident shock. Thus, rows of holes arranged in a staggered fashion can behave like a slot in its ability to block downstream information from propagating upstream via the barrier shocks. Second, in the region downstream of the incident shock, the band of minimum pressure about the holes in the spanwise direction does not have the chevron shape.

From Fig. 6, it can be seen that even when there are no incident shocks, the flow coefficient (and hence, bleed rate) increases from row 1 to 4. The increase is small from row 1 to 2 and from row 3 to 4. But, the increases from row 1 to 3 and from row 2 to 4 are more significant because of the barrier shocks in rows 1 and 2. The increases in bleed rate and flow coefficient from row 1 to 3 were found to be similar to the increase from row 2 to 4. When there is an incident shock, Fig. 6 shows that the flow coefficients in all rows were higher than those for the case without the incident shock. For cases 1 and 2, the difference indicates that the high pressure downstream of the incident shock did propagate upstream through the subsonic part of the boundary layer, though not appreciably. For cases 1, 3, and 4, the differences in the flow coefficients are also due to different spacings between holes. Figure 6 also showed that the flow coefficients increase considerably from row 1 to 3 and from row 2 to 4. This, of course, is primarily due to the markedly increased pressures created by the incident shock.

Effects of Hole Arrangement

The effects of the angle θ on shock-wave/boundary-layer interactions with bleed can be seen by examining the results for cases 2 and 4. In case 2, the angle θ is equal to 60 deg, and in case 4, that angle is equal to 70 deg. Note that for both cases, $L_y = D$, so that the distance between rows (L_x) for case 4 is greater than that for case 2. Also, note that for both cases, the third row is positioned at $13D$ from the inflow boundary (see Fig. 1). From Fig. 5, it can be seen that case 4 has larger regions with adverse pressure gradients than case 2. This is expected since the distance between rows is increased. Though this implies that case 4 is less resistant to flow separation than case 2, flow separation did not take place for either of these cases. This indicates that rows can be spaced further apart in the streamwise direction and still be able to control boundary-layer separation. With a larger separation distance, fewer bleed holes would be needed to span a given streamwise length, which would reduce the overall amount of bleed.

The effects of the distance between bleed holes for a given angle θ can be seen by examining the results for cases 2 and 3. For both of these cases, the angle θ is equal to 60 deg, but L_y equals D for case 2 and $1.5D$ for case 3. Also, for both cases, the third row is positioned at $13D$ from the inflow boundary (see Fig. 1). By having L_y greater than D it is possible for information downstream of the incident shock to propagate upstream between the bleed holes along the

streamwise direction without having to "wind" around the holes as in cases 1, 2, and 4. From Fig. 5 (case 3), it can be seen that this is not the situation, however. Though the upstream influence due to the incident shock is greater for case 3 than case 2, the holes in row 2 still effectively blocked the shock-induced adverse pressure gradient from propagating further upstream. This blockage was able to prevent flow separation for case 3.

Case 3 can also be compared with case 4 since these two cases have the same L_x, but different L_y. Comparing these two cases in Fig. 5 shows that with a larger L_y, the upstream influence length is longer. With a longer upstream influence length, the region of minimum pressure between the bleed holes in the spanwise direction is no longer connected. However, as noted earlier, the configuration represented by case 3 was still able to block effectively the shock-induced adverse pressure gradient and prevent flow separation. This is because bleed causes the boundary-layer profiles just downstream of a hole to be fuller, and this fuller profile can withstand a larger region of adverse pressure gradient. Thus, both L_x and L_y, can exceed D. The spacing of the holes should depend on the boundary-layer profile created by bleed and on the amount of adverse pressure gradient that profile can withstand in order to control flow separation with minimum bleed.

Figure 6 shows the following effects of bleed-hole arrangement on bleed rate and flow coefficient. First, bleed rate and flow coefficient are strong functions of L_x. This can be seen by comparing these two parameters in cases 2 and 4, which shows that the higher the value of L_x, the higher are the bleed rate and flow coefficient. Second, the effect of L_y on bleed rate and flow coefficient is less than that of L_x. This can be seen by comparing these two parameters in cases 3 and 4.

Concluding Remarks

This three-dimensional computational study showed how θ, the distance between bleed holes, and whether an incident shock strikes the boundary layer or not affect shock-wave/boundary-layer interactions on a flat plate with bleed. Based on this study, the following conclusions can be made. First, a barrier shock forms in every hole by the bleed process itself if the plenum pressure is sufficiently low. Second, these barrier shocks induce considerable disturbances above the plate. Third, when there are rows of holes arranged in a staggered fashion, bleeding through these holes exerts considerable spanwise influence. Fourth, for the bleed-hole spacings investigated, only two rows of holes were needed to block the shock-induced adverse pressure gradient from propagating upstream. This indicates that judicious hole placement can greatly reduce the amount of bleed needed to control flow separation. Fifth, both L_x and L_y can exceed D with the optimum value dependent upon the boundary-layer profile created by bleed and on the amount of adverse pressure gradient that profile can withstand before separating. This indicates that further optimization can be made by minimizing bleed per unit area.

Acknowledgments

This work was supported by Cooperative Agreement NCC2-845 from NASA Ames Research Center. The computer time was provided by the NAS facility. The authors are grateful for this support.

References

[1]Delery, J. M., "Shock Wave/Turbulent Boundary Layer Interaction and Its Control," *Progress in Aerospace Sciences*, Vol. 22, 1985, pp. 209–280.

[2]Hamed, A., and Shang, J., "Survey of Validation Data Base for Shockwave Boundary Layer Interactions in Supersonic Inlets," *Journal of Propulsion and Power*, Vol. 7, No. 4, 1991, pp. 617–625.

[3]Abrahamson, K. W., and Bower, D. L., "An Empirical Boundary Condition for Numerical Simulation of Porous Plate Bleed Flows," AIAA Paper 88-0306, Jan. 1988.

[4]Chyu, W. J., Howe, G. W., and Shih, T. I-P., "Bleed Boundary Conditions for Numerically Simulated Mixed-Compression Supersonic Inlet Flows," AIAA Paper 88-0270, Jan. 1988; also *Journal of Propulsion and Power*, Vol. 8, No. 4, 1992, pp. 862–868.

[5]Benhachmi, D., Greber, I., and Hingst, W., "Experimental and Numerical Investigation of an Oblique Shock Wave/Boundary Layer Interaction with Continuous Suction," AIAA Paper 89-0357, Jan. 1989.

[6]Paynter, G. C., Treiber, D. A., and Kneeling, W. D., "Modeling Supersonic Inlet Boundary Layer Bleed Roughness," *Journal of Propulsion and Power*, Vol. 10, No. 4, 1994, pp. 622–627.

[7]Lee, J., Sloan, M. L., and Paynter, G. C., "Lag Model for Turbulent Boundary Layers Developing over Rough Bleed Surfaces," *Journal of Propulsion and Power*, Vol. 10, No. 4, 1994, pp. 562–568.

[8]Hamed, A., and Lehnig, T., "Investigation of Oblique Shock/Boundary Layer/Bleed Interaction," *Journal of Propulsion and Power*, Vol. 8, No. 2, 1992, pp. 418–424.

[9]Hamed, A., and Lehnig, T., "Effect of Bleed Configuration on Shock/Laminar Boundary-Layer Interactions," *Journal of Propulsion and Power*, Vol. 11, No. 1, 1995, pp. 42–48.

[10]Hamed, A., Shih, S. H., and Yeuan, J. J., "An Investigation of Shock/Turbulent Boundary Layer/Bleed Interactions," AIAA Paper 92-3085, July 1992.

[11]Hamed, A., Shih, S. H., and Yeuan, J. J., "A Parametric Study of Bleed in Shock Boundary Layer Interactions," AIAA Paper 93-0294, Jan. 1993.

[12]Hamed, A., Yeuan, J. J., and Shih, S. H., "An Investigation of Shock Wave Turbulent Boundary Layer Interactions with Bleed Through Slanted Slots," AIAA Paper 93-2992, July 1993.

[13]Hahn, T. O., Shih, T. I-P., and Chyu, W. J., "Numerical Study of Shock-Wave/Boundary-Layer Interactions with Bleed," *AIAA Journal*, Vol. 31, No. 5, 1993, pp. 869–876.

[14]Omi, J., Shiraishi, K., Sakata, K., Murakami, A., Honami, S., and Shigematsu, J., "Two-Dimensional Numerical Simulation for Mach-3 Multishock Air-Intake with Bleed Systems," AIAA Paper 93-2306, June 1993.

[15]Rimlinger, M. J., Shih, T. I-P., and Chyu, W. J., "Three-Dimensional Shock-Wave/Boundary-Layer Interactions with Bleed Through a Circular Hole," AIAA Paper 92-3084, July 1992.

[16]Shih, T. I-P., Rimlinger, M. J., and Chyu, W. J., "Three-Dimensional Shock-Wave/Boundary-Layer Interaction with Bleed," *AIAA Journal*, Vol. 31, No. 10, 1993, pp. 1819–1826.

[17]Chyu, W. J., Rimlinger, M. J., and Shih, T. I-P., "Control of Shock-Wave/Boundary-Layer Interactions by Bleed," *AIAA Journal*, Vol. 33, No. 7, 1995, pp. 1239–1247.

[18]Baldwin, B., and Lomax, H., "Thin Layer Approximation and Algebraic Model for Separated Turbulent Flows," AIAA Paper 78-257, Jan. 1978.

[19]Buning, P. G., and Chan, W. M., *OVERFLOW/F3D User's Manual*, NASA Ames Research Center, Moffett Field, CA, 1991.

[20]Steger, J. L., and Warming, R. F., "Flux-Vector Splitting of the Inviscid Gasdynamic Equations with Application to Finite-Difference Methods," *Journal of Computational Physics*, Vol. 40, No. 2, 1981, pp. 263–293.

[21]Steger, J. L., Ying, S. X., and Schiff, L. B., "A Partially Flux-Split Algorithm for Numerical Simulation of Compressible Inviscid and Viscous Flow," *Proceedings of the Workshop on Computational Fluid Dynamics*, Inst. of Nonlinear Sciences, Univ. of California, Davis, CA, 1986.

[22]Benek, J. A., Buning, P. G., and Steger, J. L., "A 3-D Chimera Grid Embedding Technique," AIAA Paper 85-1523, July 1985.

[23]Rimlinger, M. J., Shih, T. I-P., and Chyu, W. J., "Three-Dimensional Shock-Wave/Boundary Layer Interactions with Bleed Through Multiple Holes," AIAA Paper 94-0313, Jan. 1994.

AIAA-96-0432

Computations of Shock-Wave/Boundary-Layer Interactions with Bleed

Mark J. Rimlinger and Tom I-P. Shih
Carnegie Mellon University
Pittsburgh, PA

Wei J. Chyu
NASA Ames Research Center
Moffett Field, CA

Brian P. Willis and David O. Davis
NASA Lewis Research Center
Cleveland, OH

34th Aerospace Sciences Meeting & Exhibit
January 15-18, 1996 / Reno, NV

AIAA 96-0432

Computations of Shock-Wave/Boundary-Layer Interactions with Bleed

M. J. Rimlinger+ and T. I-P. Shih++
Carnegie Mellon University, Pittsburgh, Pennsylvania

W. J. Chyu#
NASA - Ames Research Center, Moffett Field, California

B.P. Willis¶ and D.O. Davis¶
NASA - Lewis Research Center, Cleveland, Ohio

ABSTRACT

Computations were performed to investigate three-dimensional, shock-wave/boundary-layer interactions on a flat plate with bleed through eight rows of normal circular holes arranged in a staggered fashion under choked conditions. The focus of the computations was to assess the usefulness of two turbulence models -- Baldwin-Lomax and Baldwin-Barth -- and issues related to grid distribution by comparing predicted results with experimental data.

This study is based on the ensemble-averaged conservation equations of mass, momentum (compressible Navier-Stokes), and total energy. As mentioned, two turbulence models were used. Solutions to the conservation equations were obtained by a diagonalized ADI scheme with central differencing and blended second- and fourth-order artificial dissipation on a Chimera overlapping grid.

+ Graduate Student, Dept. of Mechanical Engineering.

++ Professor, Dept. of Mechanical Engineering. Senior Member AIAA.

Research Scientist, Applied Aerodynamics Branch. Member AIAA.

¶ Research Engineer, Inlet, Duct, and Nozzle Flow Physics Branch. Member AIAA.

INTRODUCTION

Effective control of shock-wave/boundary-layer interactions is essential to the successful operation of a wide variety of aerodynamic and propulsion devices. These devices include mixed-compression supersonic inlets, transonic wind tunnels, and airframe of supersonic aircraft. Supersonic or transonic flows through such devices usually exhibit shock waves generated by geometrical changes or back pressure constraints. The adverse pressure gradients created by these shock waves cause flow distortion, and if sufficiently strong, can also cause flow separation[1] with the latter often leading to highly detrimental effects on performance.

One widely used method for controlling detrimental effects of shock-wave/boundary-layer interactions is bleed. Control through bleed consists of placing holes or slots in vicinities where shock waves impinge on the boundary layer. These bleed holes, being connected to one or more plenums at lower pressures, remove the low momentum fluid next to the wall so that the remaining boundary layer, having higher momentum, can now withstand the adverse pressure gradient without separating. Although bleed is an effective method of control, it has associated penalties. In the case of supersonic mixed-compression inlets, removal of boundary layer fluid reduces mass flow for propulsion, decreases total pressure recovery, and increases drag because of the need to vent bled air into the freestream. Thus the designer must try to bring

about the most effective control with the least amount of bleed.

The importance of bleed in controlling shock-wave/boundary-layer interactions has led a number of investigators to use both experimental and computational methods to study this problem[1-15]. Computational studies -- if they can be validated -- are of particular interest because they have the potential to reveal considerable details about the flowfield and they can be used as a design tool. Recently, Willis, et al.[15] reported detailed measurements of pitot-stagnation-pressure profiles at several stations in a shock-wave/boundary-layer/bleed interaction problem which can be used to validate computations. Thus, the objective of this investigation is to compute the problem studied by Willis, et al. with focus on validation. Other computational issues touched upon include the turbulence model used and grid distribution.

In the next section, the problem studied is described in detail. Afterwards, the formulation, numerical method of solution, and results obtained are presented.

DESCRIPTION OF PROBLEM

The problem investigated by Willis, et al.[9] is shown in Fig. 1. Since our interest is in the region about the bleed holes, the domain was contracted to render it tractable but in a way that would still capture the essence of the original problem. The contracted problem is shown schematically in Fig. 2 (not drawn to scale).

The problem studied involves a supersonic turbulent boundary layer flow on a flat plate with an embedded incident and reflected shock wave, bleed of the boundary layer through eight rows of circular holes drilled vertically in the plate and arranged in a staggered fashion, and a plenum where the bled air is discharged. For this problem, the domain is the region bounded by the dashed lines which includes the region above the flat plate, the plenum, and the eight "half" bleed holes. Only eight "half" bleed holes needed to be included in the domain because of the symmetry in the spanwise direction.

The physical dimensions of this problem are as follows (see Fig. 2): All bleed holes have the same diameter D (0.635 cm). Bleed holes between adjacent rows and columns are spaced D apart in the spanwise direction (y-coordinate) and 2D apart in the streamwise direction (x-coordinate) -- measured from hole centers. The flat plate has a thickness of D. The length (L) and height (H) of the region above the flate plate are 36.47 cm and 15.9 cm, respectively. The plenum dimensions, L_p and H_p, are 13.65 cm and 10 cm, respectively. The edge of the first row of bleed holes is L_b (8.2 cm) downstream of the inflow boundary. The shock-wave generator is located at a distance L_s upstream of the inflow boundary so that the incident shock wave would impinge on the flate plate midway between the fourth and the fifth row of bleed holes if the flow above the plate had a uniform profile. α was set equal to 8° which produced an incident shock wave that was strong enough to induce flow separation on the flat plate in the absence of bleed.

The flow conditions for this problem are as follows: The fluid that enters the domain above the flat plate is air with a constant specific-heats ratio (γ) of 1.4. The freestream Mach number (M_∞), stagnation pressure (P_o), and stagnation temperature (T_o) are 2.46, 172.36 KPa, and 291.6 K, respectively. This supersonic flow has a turbulent, boundary layer next to the flat plate. At the inflow boundary, this boundary layer has a thickness of 2.63 cm (or 4.14D), a displacement thickness of 0.727 cm, a momentum thickness of 0.196 cm, and a friction factor of 1.43×10^{-3}. To induce flow of air through the bleed holes, the back pressures (P_b) at the exit of the plenum was set at $0.0321P_o$ which caused the flow through the bleed holes to be choked.

FORMULATION OF PROBLEM

The flow problem described in the previous section was modelled by the density-weighted, ensemble-averaged conservation equations of mass, momentum ("compressible" Navier-Stokes), and total energy written in generalized coordinates and cast in strong conservation-law form. Two different turbulence models were used. One model is the Baldwin-Lomax algebraic turbulence model[16]. The other is the Baldwin-Barth one-equation model[17]. Since the conservation equations and the turbulent models used are well documented in the literature, additional details are not given.

In order to obtain solutions to the conservation equations, boundary and initial conditions are needed. The boundary conditions (BCs) employed in this study for the different boundaries shown in Fig. 2 are as follows. At the inflow boundary where the flow is supersonic everywhere except for a very small region next to the flat plate, two types of BCs were imposed. Along segment A-B, all flow variables were specified at the freestream condition except those in the region containing the boundary layer. In the boundary layer, the pitot-stagnation-pressure profile measured by Willis, et al. was used to compute a velocity profile by assuming constant static pressure in the boundary layer and using the Rayleigh supersonic pitot formula in the supersonic region and isentropic relations in the subsonic region[18]. The static temperature profile in the boundary layer was computed by using the adiabatic Crocco-Busemann relation[19] with a recovery factor of 0.89. The remaining quantities needed in the boundary layer readily follow from constitutive relations. Along segment B-C, post-shock conditions based on inviscid, oblique, shock-wave theory were specified. These post-shock conditions were also specified along the freestream boundary (segment C-D).

At the outflow boundary where the reflected shock wave exited the computational domain, the flow is also mostly supersonic except for a small region next to the flat plate so that all flow variables were extrapolated. Here, linear extrapolation based on three-point, backward differencing was employed. The BCs imposed at the two symmetry boundaries were zero derivatives of the dependent variables except for the velocity component normal to those boundary which was set equal to zero. At the exit of the plenum where the flow is subsonic, a back pressure (P_b) was imposed, and density and velocity were extrapolated in the same manner as the variables at the outflow boundary. At all solid surfaces, the no-slip condition, adiabatic walls, and zero normal-pressure gradient were imposed.

Even though only steady-state solutions were of interest, initial conditions were needed because the unsteady form of the conservation equations was used. The initial conditions employed in this study were as follows. In the region above the flat plate, the initial condition was the two-dimensional, steady-state solution for an incident and a reflected oblique shock wave on a flat plate based on inviscid, oblique, shock-wave theory. The boundary layer region was modified according to that described earlier for the inflow boundary. The initial conditions used in the bleed hole and plenum were stagnant air at constant static pressure (P_b) with a density equal to the air density at the plate surface.

NUMERICAL METHOD OF SOLUTION

Solutions to the ensemble-averaged conservation equations along with the turbulence models described in the previous section were obtained by using the OVERFLOW code. The details of this code is described by Buning and Chan[20]. The OVERFLOW code contains many algorithms. The one used in this study is as follows: All convection and diffusion terms were centrally differenced with a blended second- and fourth-order artificial dissipation function added to maintain numerical stability. The time-derivative terms were approximated by the Euler implicit formula since only steady-state solutions were of interest. The system of nonlinear equations that resulted from the aforementioned approximations to the space- and time-derivatives were analyzed by using a diagonalized ADI scheme[21]. In OVERFLOW, Jacobians and metric coefficients are interpreted as grid-cell volumes and grid-cell surface areas, respectively. In this regard, all algorithms in OVERFLOW are implemented in the finite-volume manner. However, BCs in OVERFLOW are implemented in a finite-difference manner in order to enhance flexibility and ease in investigating different problems.

For the bleed-hole problem shown in Fig. 2, the computational domains were always divided into 18 zones -- one above the plate, two for each of the eight bleed holes, and one for the plenum. For this 18-zone computational domain, a Chimera overlapped grid system was employed. An example of the Chimera grid system used is shown in Figs. 3 and 4. For the zone above the flat plate, the grid system used was a single solution-adapted H-H grid (adaptation was based on the initial conditions) which has grid points clustered near the flat plate, bleed holes, and the impinging and reflected shock waves (Fig. 3). The number of grid lines used in this H-H grid is as follows: either 351 or 595 from inflow to

outflow, 201 from plate surface to freestream boundary, and 23 between the two symmetry boundaries.

For each zone containing a bleed hole, two overlapping grids were used -- an O-H grid touching the wall of the bleed hole and an H-H grid at the center of the bleed hole (Fig. 4). The O-H grid with 125 x 47 x 27 grid points is used to resolve the circular geometry of the bleed hole. The H-H grid with 125 x 11 x 19 grid points is used to eliminate the centerline singularity associated with the O-H grid. Note that the grids in the bleed hole overlap the grid in the plenum and the grid above the flat plate. The reason for extending the bleed-hole grids further into the plenum is to accelerate convergence rate to steady-state[13].

For the zone containing the plenum, a single H-H grid was used (Fig. 3). This H-H grid has either 275 x 55 x 23 or 495 x 55 x 23 grid points. The grid points are clustered near walls and the bleed holes.

The grid system described above was generated by using algebraic grid generation with one-dimensional stretching functions. Note that grid spacings in different grids were made comparable in regions where they overlapped in order to minimize aliasing errors. Also, note that two different grid systems were used for the plate and plenum -- one with fewer points (henceforth referred to as the coarse mesh) and one with almost double the number of points in the streamwise direction (henceforth referred to as the fine mesh).

During computations, the flowfield in each grid was analyzed one at a time in the following order: (i) the H-H grid above the flat plate, (ii) the H-H grid in the bleed hole, (iii) the O-H grid in the bleed hole, (iv) repeat ii and iii for all bleed holes, and (v) the H-H grid in the plenum. Information from one grid was passed to another grid via trilinear interpolation at grid boundaries. The required interpolation coefficients were obtained by using the PEGSUS code[22]. This process of analyzing the flow in one grid at a time until all grids are analyzed was repeated for each time step until a converged solution was obtained. Typically, 3000 time steps or iterations are needed in order to obtain a converged solution. The amount of CPU time needed on a Cray C-90 is about 16 hours for the coarse mesh and 30 hours for the fine mesh

RESULTS

Numerical solutions were performed to investigate the shock-wave/boundary-layer/bleed interaction problem of Willis, et al.[15] focusing on validation. Since the accuracy of the computations is a strong function of both the turbulence model and the grid distribution, these two issues are touched upon. A summary of the cases studied is given in Table 1. Cases were run with and without bleed for two different turbulence models: Baldwin-Lomax and Baldwin-Barth. For the cases with bleed, solution were obtained by using a coarse grid and a fine grid.

Table 1. Summary of Cases Studied

Case No.	Bleed?	Turbulence Model	Grid
1	No	Baldwin-Lomax	Coarse
2	No	Baldwin-Barth	Coarse
3	Yes	Baldwin-Lomax	Coarse
4	Yes	Baldwin-Barth	Coarse
5	Yes	Baldwin-Lomax	Fine

Table 2. Bleed Rates (kg/s)

Baldwin-Lomax (coarse mesh)	Baldwin-Barth (coarse mesh)	Exp.
0.0781	0.0826	0.0885

Results for this study are given in Table 2 and Figs. 5 to 11. Table 2 gives the computed and the measured bleed rates in which the computed results were obtained by using the coarse mesh. Figures 5 and 6 show a side view (i.e., the x-y plane passing through section a-b in Fig. 2) of the Mach number and pressure contours for Case 3. Figures 7 and 8 show a side view of the Mach number and pressure contours in the region about the bleed holes with and without bleed (Cases 2 to 4). Figure 9 shows a top view (i.e., x-y plane) of the pressure contours on the plate surface.

Finally, Figs. 10 and 11 compare the predicted pitot-stagnation-pressure profiles against the values measured by Willis, et al.[15] These results are described below along with results for Case 5 which are not shown because they are qualitatively similar to those of Cases 3 and 4.

General Features of the Flow To provide a framework for the discussion on turbulence models, grid distributions, and validation, the overall flow features are briefly described. From Figs. 5 and 6, it can be seen that the incident and reflected shock waves were captured relatively crisply by the solution-adapted coarse mesh. From these two figures, one can also see the bleed-generated barrier shocks emanating from the bleed holes and extending upwards through the boundary layer -- creating a wave-like boundary-layer edge over the bleed region. Figures 5 to 8, 10, and 11 show how the barrier shock affect both the incident and the reflected shocks. In particular, note the waviness in the pitot-stagnation pressure profile at the stations near x= 10.0 cm and 13.5 cm in Fig. 10.

Figures 5 to 8 also show the choked flow in the bleed holes as well as the jet-like flow in the plenum issuing from the bleed holes. Jets from bleed holes upstream of the incident and reflected shocks do not seem to interact with each other appreciably. Jets from bleed holes downstream of the incident and reflected shocks, however, do have significant interaction. This enhanced interaction is due to the significantly higher mass flow rates through these holes.

From Figs. 7(a) and 8(a), one can see that, in the absence of bleed, the incident shock wave is sufficiently strong to induce a large separated region on the flat plate. The results shown in Figs. 7(a) and 8(a) for the no bleed case were computed by using the Baldwin-Barth turbulence model (Case 2).

Most of the flow features described above have been reported in Refs. 5, 7, 12, and 13. Readers are referred to these references for further information.

Effects of Turbulence Model and Grid Distribution One focus of this study is to touch upon the effects of turbulence model and grid distribution on the computed results. In the following, we discuss these two aspects without reference to the experimental data. The experimental data of Willis, et al.[15] will be referred to and compared against in the subsection on validation.

From Figs. 7 to 9 and Table 2, one can see the differences between the results obtained by the Baldwin-Lomax (B-L) and the Baldwin-Barth (B-B) models. The most important difference is the predicted extent of flow separation. The B-B model predicted a larger separation bubble than did the B-L model. The separation bubbles of interest are those located in a region on the flat plate between the third and the fifth row of bleed holes (Fig. 9). The formation of these separation bubbles are due to the adverse pressure gradient created by the incident shock. The prediction of a larger separated region by the B-B model has significant implications. With a larger separation bubble, the reflected shock is shifted upstream (see pitot stagnation-pressure profile at stations near x = 7.5 cm and 10 cm in Fig. 10). This shift exposes more bleed holes to higher static pressures which increases the bleed rate (Table 2).

Another difference between the two turbulence models is the predicted pitot-stagnation-pressure profiles downstream of the bleed region as shown in Fig. 11. From this figure, it can be seen that, the B-L model gives a much fuller profile with higher pitot-stagnation pressure near the wall than does the B-B model (see profiles at station near x = 25.0 cm in Fig. 11). Since these profiles are used to evaluate flow distortion, it can be seen that the turbulence model used can make a considerable difference. These predictions are described in more detail in the next sub-section.

To discuss the effects of grid distribution on the computed results, recall that both the coarse and the fine meshes have the same number of grid points in the bleed holes. They differ only in the plenum and above the plate, and that difference is in the number of grid points along the streamwise direction and not in the normal direction. In the normal direction, both the coarse and the fine meshes have grid points highly clustered to the flat plate ($y^+ \leq 1$ for the first point away from the wall). With that as a backdrop, it was found that with more grid points in the streamwise direction, the B-L model predicted a larger separation bubble with size similar to that predicted by the B-

B model on the coarse mesh. With a larger separation bubble, the reflected shock shifted upstream, and the bleed rate increased. Here, it is noted that with the larger separation bubble, the pitot-stagnation-pressure profiles also changed downstream of the bleed region, and agreed better with the measured values than did the B-B model.

Validation In this section, the quality of the computations is evaluated by comparing the predicted pitot-stagnation-pressure profiles against the measured ones reported by Willis, et al.[15] The predicted and measured bleed rates are also compared. These comparisons are given in Figs. 10 and 11 and in Table 2 for the coarse mesh. See Fig. 1 to get an appreciation for the relative locations in the flow domain where pitot-stagnation-pressure pro-files are compared. The bleed region is between x = 0 and x = 9.525 cm.

From Figs. 10 and 11, it can be seen that the pitot-stagnation-pressure profiles predicted by both the B-L and the B-B models are in good agreement with experimental data upstream of the incident shock. In the region about the incident and the reflected shocks, these figures show that the B-B model was able to predict correctly the position of the reflected shock, whereas the B-L model was not (see profiles at stations near x = 7.5 cm and 10 cm). This is because the B-B model predicted correctly the size of the separation bubble which shifted the reflected shock upstream. Since the position of the reflected shock depends on both the bleed-generated barrier shocks and the separation bubbles on the surface (if they exist), bleed-boundary-condition models must account for these aspect in order to predict accurately the reflected shock positions.

Downstream of the bleed region, the B-L model accurately predicted the pitot-stagnation-pressure profiles, but the B-B model did not. The B-B model could not recover from the shock-wave/boundary-layer interaction region because the physics needed to describe it was not built into the model. Since the B-L model assumes the production of turbulence to be equal to its dissipation, the accurate results generated by this model downstream of the bleed region indicate that the flow there is essentially in equilibrium as far as turbulence quantities are concerned.

Since the B-B model predicted the size of the separation bubble better, it also predicted the bleed rate more accurately (see Table 2). Recall that the further upstream the reflected shock lies, the higher the bleed rate.

When the number of grid points was increased for the B-L model, this model was also able to predict correctly the size of the separation bubble and position of the reflected shock. But, for this fine mesh computation, the predicted pitot-stagnation-pressure profiles downstream of the bleed region were less satisfactory. It seems that with the B-L model, if the separation bubble exceeds a certain size, then its predictions become less acceptable. However, if the flow does not separate above the plate, then the B-L model gives accurate results for the problem involving shock-wave/boundary-layer interactions with bleed.

SUMMARY

Computations were performed to assess the usefulness of two turbulence models -- Baldwin-Lomax and Baldwin-Barth -- and issues related to grid distribution by comparing predicted results with experimental data. Computations show that Baldwin-Lomax (B-L) can produce accurate results for bleed rate as well as the boundary layer (BL) pitot-stagnation-pressure profiles with a relatively coarse grid provided separation bubbles on the flat plate are either non-existent or very small. With a finer grid, B-L predicted a larger separation bubble. But, once B-L predicts a separation bubble that is sufficiently large, then results predicted downstream of it become less satisfactory. If B-L does not predict separation though one exists, then the predicted bleed rate will be lower than should be, but the predicted pitot-stagnation pressure downstream of the bleed region will be accurate. Though B-B can predict flow separation on the flat plate with a relatively coarse grid, it too does not provide satisfactory results for this problem if there is flow separation.

ACKNOWLEDGEMENT

This work was supported by NASA Cooperative Agreement NCC2-845 from NASA Ames Research Center. All computations were performed at NAS Facility. The authors are grateful for this support.

REFERENCES

1. Delery, J.M., "Shock Wave / Turbulent Boundary Layer Interaction and Its Control," Progress in Aerospace Sciences, Vol. 22, 1985, pp. 209-280.

2. Hamed, A. and Shang, J., "Survey of Validation Data Base for Shockwave Boundary Layer Interactions in Supersonic Inlets," AIAA Journal of Propulsion and Power, Vol. 7, No. 4, 1991, pp. 617-625.

3. Benhachmi, D. Greber, I., and Hingst, W., "Experimental and Numerical Investigation of an Oblique Shock Wave / Boundary Layer Interaction with Continuous Suction," AIAA Paper 89-0357, January 1989.

4. Hamed A. and Lehnig, T., "Investigation of Oblique Shock/Boundary Layer/Bleed Interaction," AIAA Journal of Propulsion and Power, Vol. 8, No. 2, 1992, pp. 418-424.

5. Rimlinger, M.J., Shih, T.I-P., and Chyu, W.J., "Three-Dimensional Shock-Wave/Boundary-Layer Interactions with Bleed Through a Circular Hole," AIAA Paper 92-3084, July 1992.

6. Hahn, T.O., Shih, T.I-P., and Chyu, W.J., "Numerical Study of Shock-Wave/Boundary-Layer Interactions with Bleed," AIAA Journal, Vol. 31, No. 5, 1993, pp. 869-876.

7. Shih, T.I-P., Rimlinger, M.J., and Chyu, W.J., "Three-Dimensional Shock-Wave/ Boundary-Layer Interaction with Bleed," AIAA Journal, Vol. 31, No. 10, 1993, pp. 1819-1826.

8. Omi, J., Shiraishi, K., Sakata, K., Murakami, A., Honami, S., and Shigematsu, J., "Two-Dimensional Numerical Simulation for Mach-3 Multishock Air-Intake with Bleed Systems," AIAA Paper 93-2306, June 1993.

9. Paynter, G.C., Treiber, D.A., and Kneeling, W.D., "Modelling Supersonic Inlet Boundary Layer Bleed Roughness," AIAA Journal of Propulsion and Power, Vol. 9, No. 4, 1993, pp. 622-627.

10. Lee, J., Sloan, M.L., and Paynter, G.C., "A Lag Model for Turbulent Boundary Layers Developing over Rough Bleed Surfaces," AIAA Journal of Propulsion and Power, Vol. 10, No. 4, 1994, pp. 562-568.

11. Hamed, A. and Lehnig, T., "Effect of Bleed Configuration on Shock/Boundary Layer Interactions," AIAA Journal of Propulsion and Power, Vol. 11, No. 1, 1995, pp. 42-48.

12. Chyu, W.J., Rimlinger, M.J., and Shih, T.I-P., "Control of Shock-Wave/Boundary-Layer Interactions by Bleed," AIAA Journal, Vol. 33, No. 7, 1995, pp. 1239-1247.

13. Rimlinger, M.J., Shih, T.I-P., and Chyu, W.J., "Shock-Wave/Boundary-Layer Interactions with Bleed through Rows of Holes," AIAA Journal of Propulsion and Power, to appear.

14. Willis, B.P., Davis, D.O., and Hingst, W.R., "Flow Coefficient Behavior for Boundary Layer Bleed Holes and Slots," AIAA Paper 95-0031, Jan. 1995.

15. Willis, B.P., Davis, D.O., and Hingst, W.R., "Flowfield Measurements in a Normal-Hole-Bled Oblique Shock-Wave and Turbulent Boundary-Layer Interaction," AIAA 95-2885, July 1995.

16. Baldwin, B. and Lomax, H., "Thin Layer Approximation and Algebraic Model for Separated Turbulent Flows," AIAA Paper 78-257, 1978.

17. Baldwin, B.S. and Barth, T.J., "A One-Equation Turbulence Transport Model for High Reynolds Number Wall-Bounded Flows," NASA TM 102847, August 1990.

18. Liepmann, H.W. and Poshko, A., Elements of Gasdynamics, John Wiley and Sons, Inc., New York, 1957.

19. White, F.M., Viscous Fluid Flow, McGraw-Hill, Inc., New York, 1974.

20. Buning, P.G. and Chan, W.M., "OVERFLOW/F3D User's Manual," 1991.

21. Pulliam, W.R. and Chaussee, D.S., "A Diagonal Form of an Implicit Approximate-Factorization Algorithm," Journal of Computational Physics, Vol. 39, 1981, pp. 347-363.

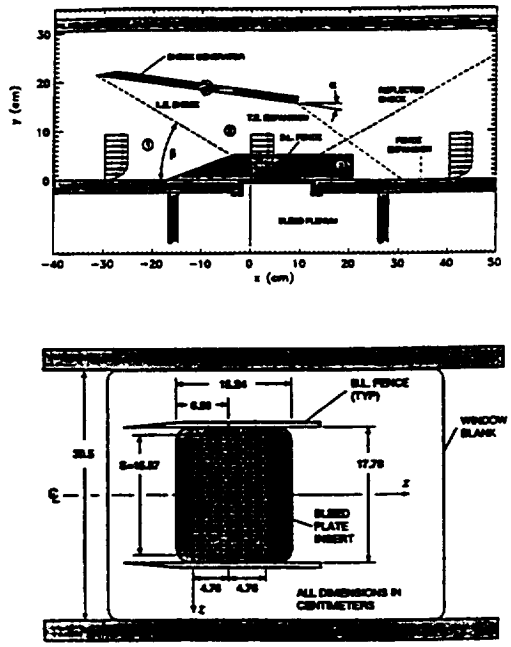

Fig. 1. Schematic diagram of problem studied by Willis, et al. (Ref. 15).

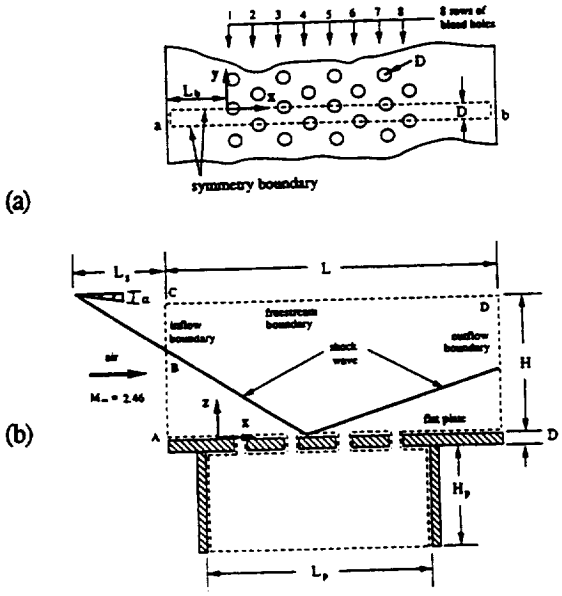

Fig. 2. Schematic diagram of problem studied. (a) Top view. (b) Side view along cross section a-b.

22. Benek, J.A., Buning, P.G., and Steger, J.L., "A 3-D Chimera Grid Embedding Technique," AIAA Paper 85-1523, 1985.

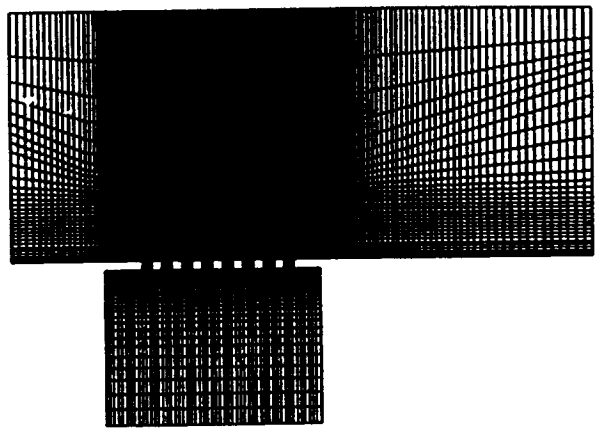

Fig. 3 Chimera overlapping grid system used (not all grid points shown).

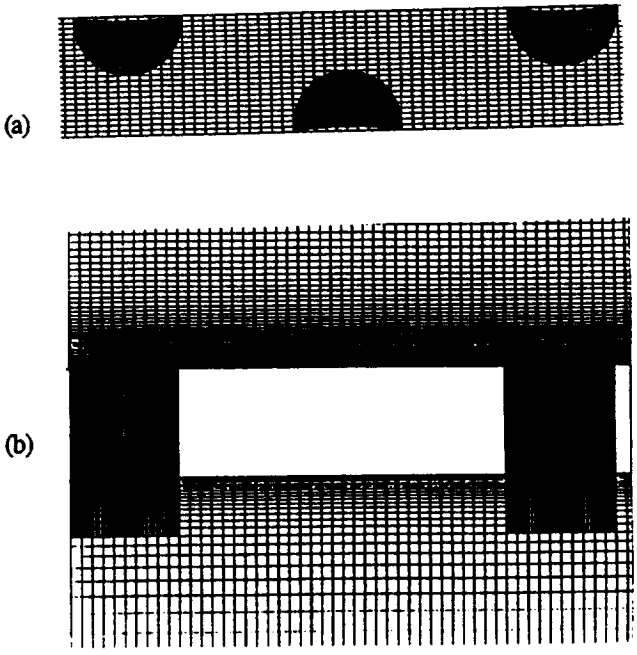

Fig. 4. Chimera grid near bleed holes. (a) Top view. (b) Side view.

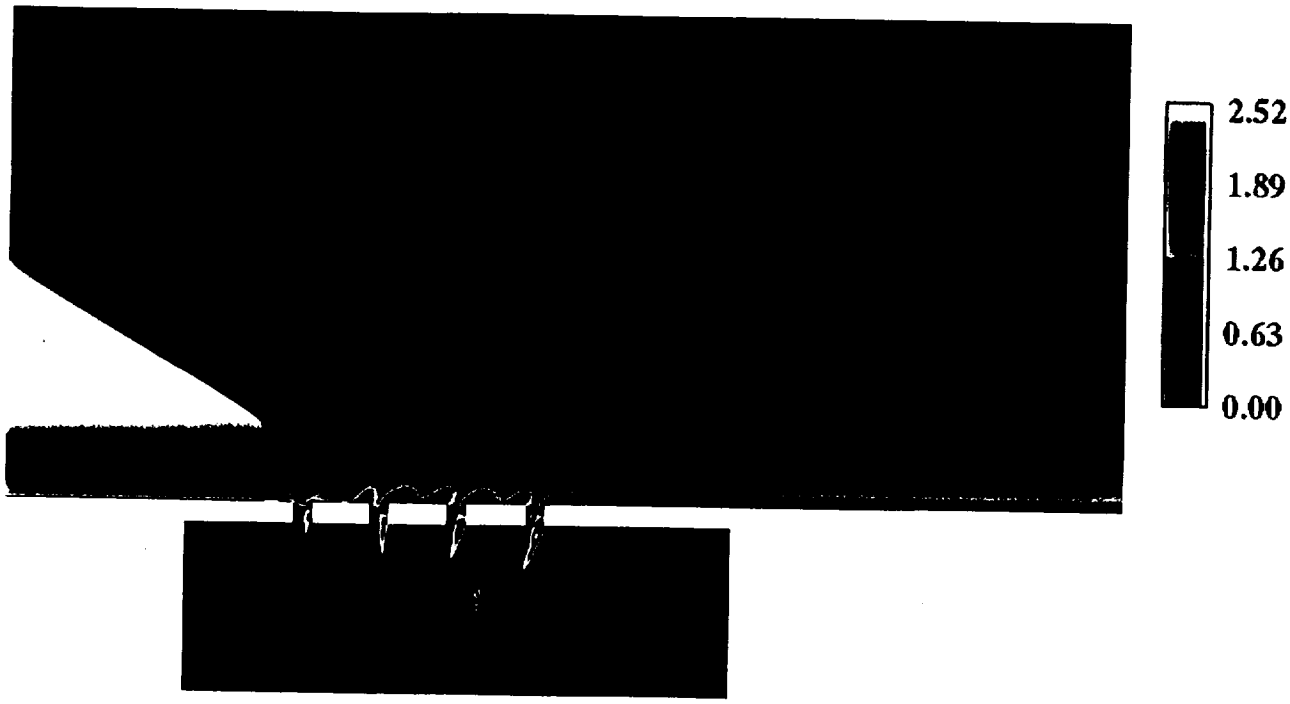

Fig. 5. Mach number contours: Baldwin–Lomax turbulence model, coarse mesh.

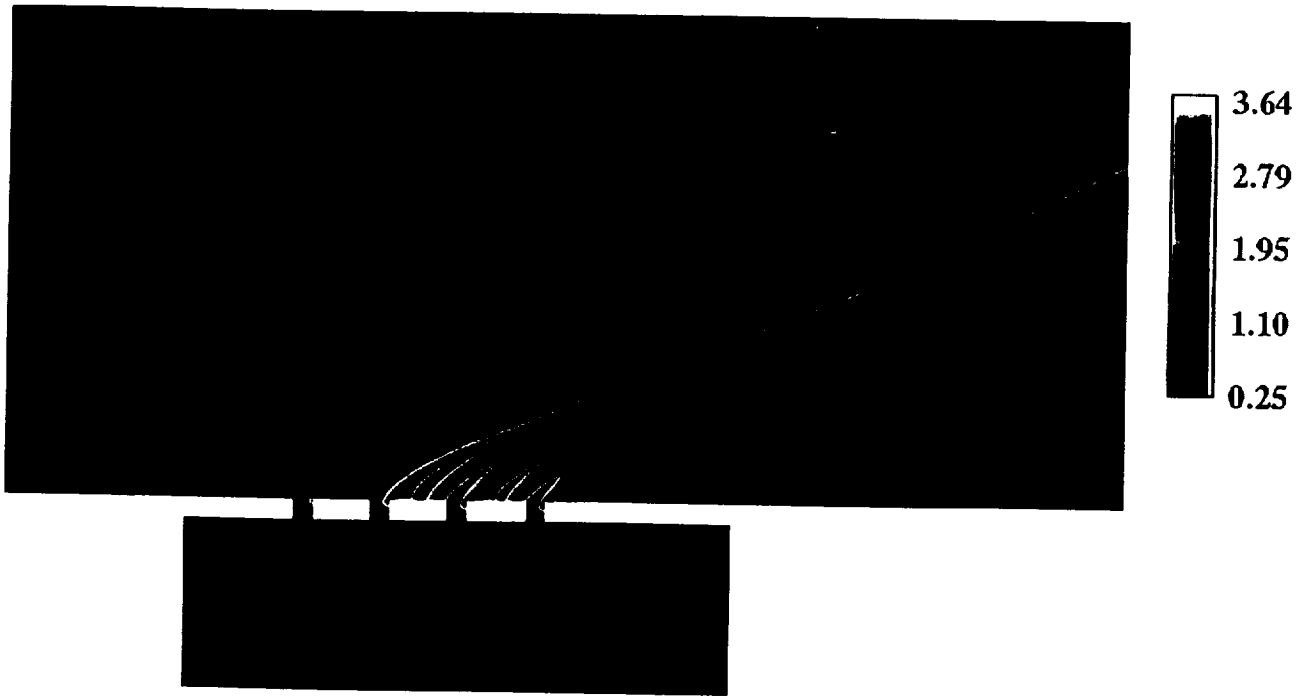

Fig. 6. Pressure contours (P/P_∞): Baldwin–Lomax turbulence model, coarse mesh.

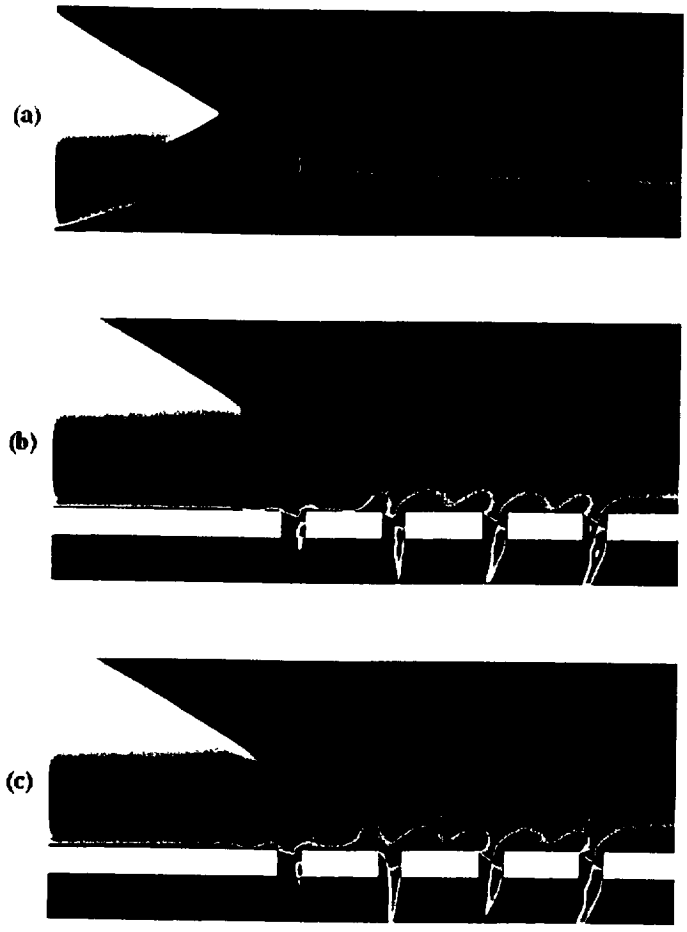

Fig. 7. Mach number contours in bleed region. See fig. 5 for scale. (a) No bleed, Baldwin–Barth. (b) Bleed, Baldwin–Lomax. (c) Bleed, Baldwin–Barth.

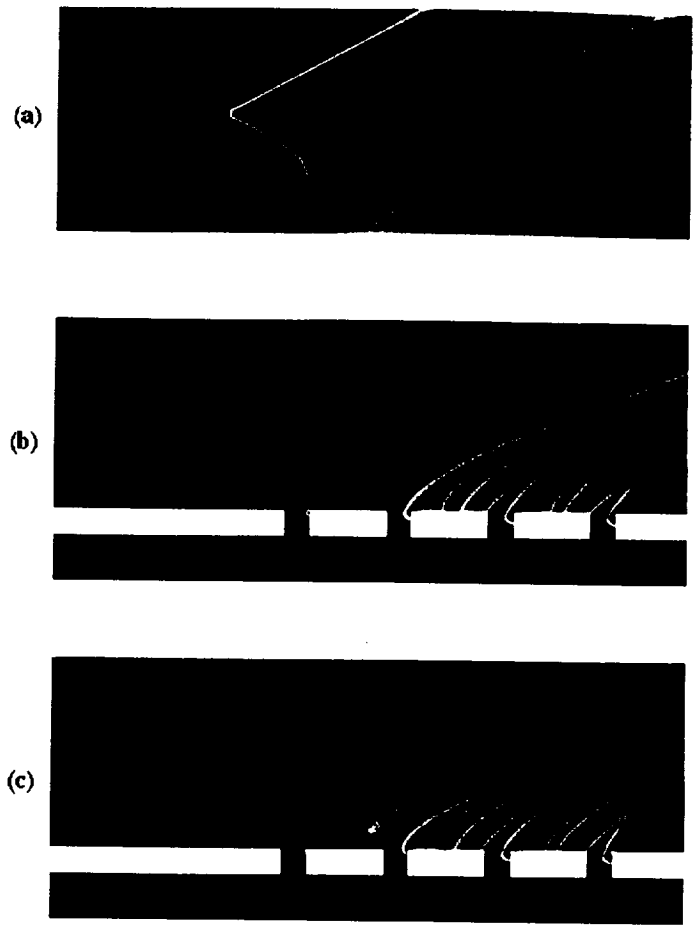

Fig. 8. Pressure contours in bleed region. See fig. 6 for scale. (a) No bleed, Baldwin–Barth. (b) Bleed, Baldwin–Lomax. (c) Bleed, Baldwin–Barth.

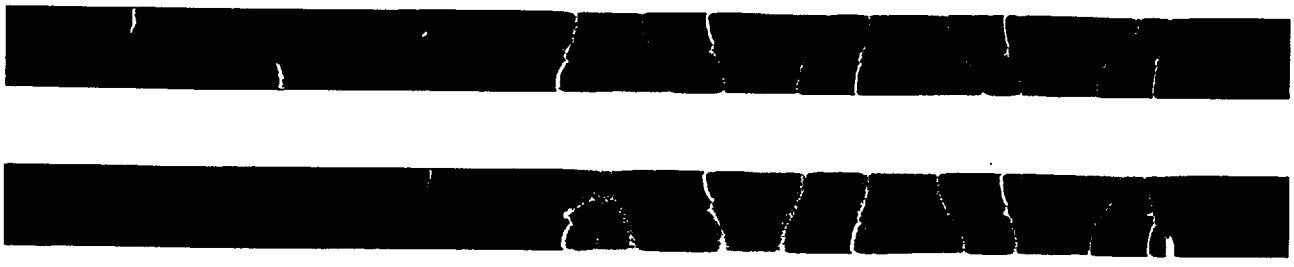

Fig. 9. Surface pressure contours in bleed region. See fig. 6 for scale. (a) Baldwin–Lomax. (b) Baldwin–Barth.

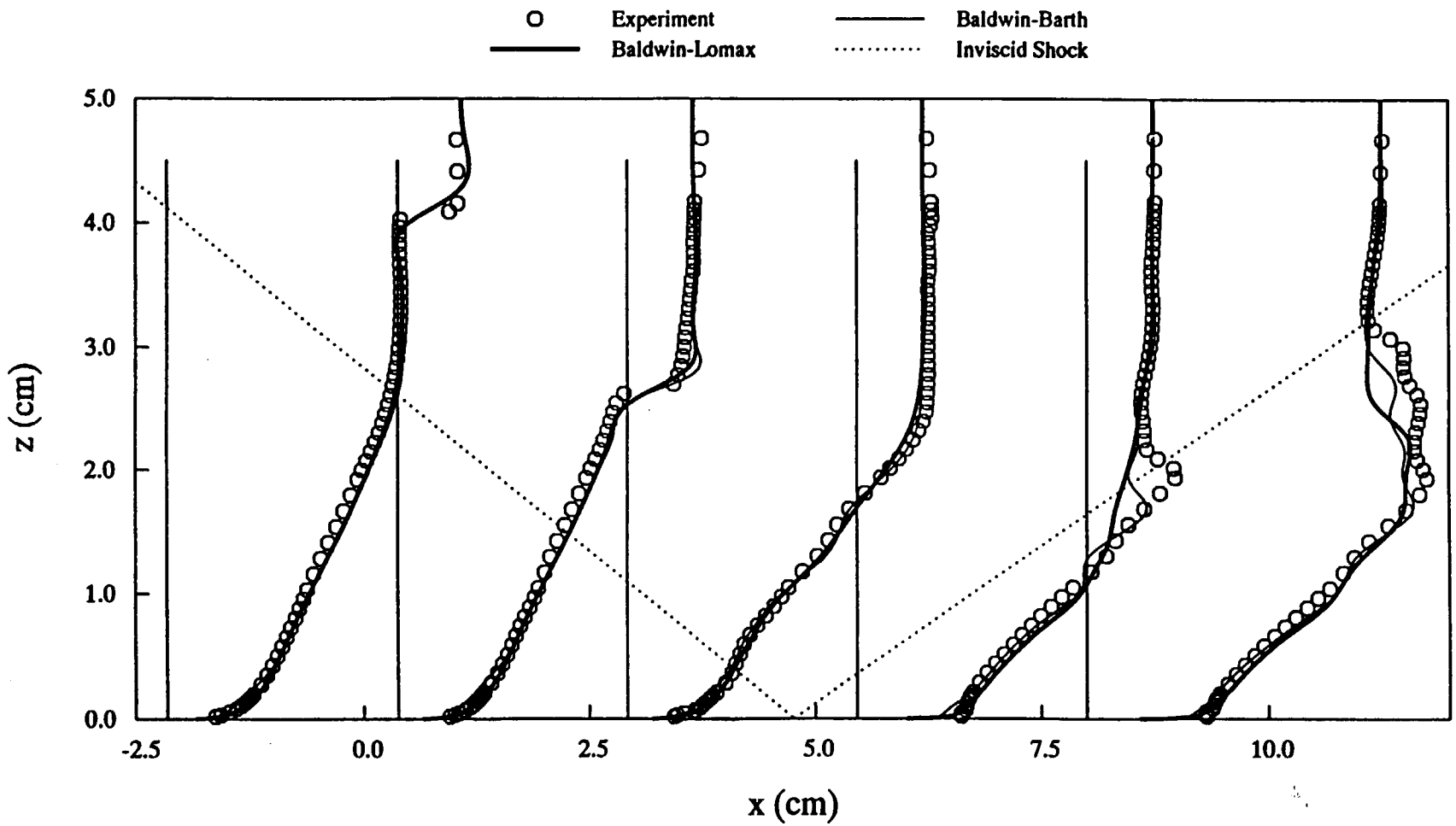

Fig. 10. Predicted and measured pitot-stagnation-pressure profiles near the bleed region.

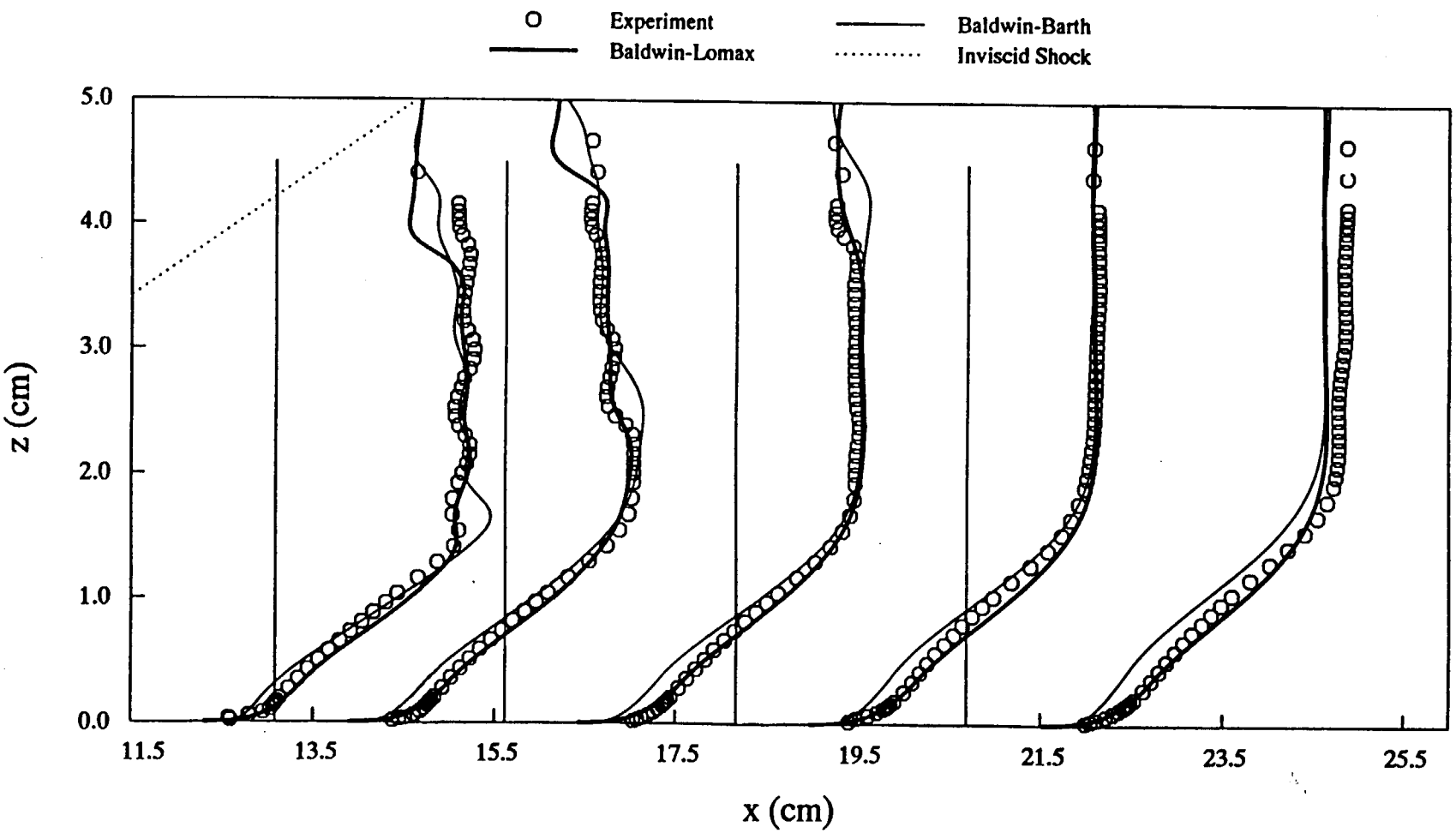

Fig. 11. Predicted and measured pitot-stagnation-pressure profiles downstream of the bleed region.